

MICROCOPY RESOLUTION TEST CHART
NATIONAL BUREAU OF STANDARDS-1963-A

(12) LEVEL III
nu

AD-E 300 725

DNA 49531

ADA 083330

DOUBLY-ASYMPTOTIC, BOUNDARY-ELEMENT ANALYSIS OF NONLINEAR SOIL-STRUCTURE INTERACTION

Lockheed Palo Alto Research Laboratory
3251 Hanover Street
Palo Alto, California 94304

30 June 1979

Final Report for Period 14 November 1977-30 June 1979

CONTRACT No. DNA 001-78-C-0026

APPROVED FOR PUBLIC RELEASE;
DISTRIBUTION UNLIMITED.

THIS WORK SPONSORED BY THE DEFENSE NUCLEAR AGENCY
UNDER RDT&E RMSS CODE B344078464 Y99QAXSC06157 H2590D.

DDC FILE COPY

Prepared for
Director
DEFENSE NUCLEAR AGENCY
Washington, D. C. 20305

DTIC
ELECTE
APR 23 1980
S D
B

80 3 14 099

Destroy this report when it is no longer
needed. Do not return to sender.

PLEASE NOTIFY THE DEFENSE NUCLEAR AGENCY,
ATTN: STTI, WASHINGTON, D.C. 20305, IF
YOUR ADDRESS IS INCORRECT, IF YOU WISH TO
BE DELETED FROM THE DISTRIBUTION LIST, OR
IF THE ADDRESSEE IS NO LONGER EMPLOYED BY
YOUR ORGANIZATION.



UNCLASSIFIED

SECURITY CLASSIFICATION OF THIS PAGE (When Data Entered)

REPORT DOCUMENTATION PAGE		READ INSTRUCTIONS BEFORE COMPLETING FORM
1. REPORT NUMBER DNA 4953F	2. GOVT ACCESSION NO. AD-A083 330	3. RECIPIENT'S CATALOG NUMBER
4. TITLE (and Subtitle) DOUBLY-ASYMPTOTIC, BOUNDARY-ELEMENT ANALYSIS OF NONLINEAR SOIL-STRUCTURE INTERACTION	5. TYPE OF REPORT & PERIOD COVERED Final Report for Period 14 Nov 77-30 Jun 79	
	6. PERFORMING ORG. REPORT NUMBER LMSD/D673964	
7. AUTHOR(s) P. G. Underwood T. L. Geers	8. CONTRACT OR GRANT NUMBER(s) DNA 001-78-C-0026	
	9. PERFORMING ORGANIZATION NAME AND ADDRESS Lockheed Palo Alto Research Laboratory 3251 Hanover Street Palo Alto, California 94304	
11. CONTROLLING OFFICE NAME AND ADDRESS Director Defense Nuclear Agency Washington, D.C. 20305	10. PROGRAM ELEMENT, PROJECT, TASK AREA & WORK UNIT NUMBERS Subtask Y99QAXSC061-57	
	12. REPORT DATE 30 June 1979	
14. MONITORING AGENCY NAME & ADDRESS (if different from Controlling Office)	13. NUMBER OF PAGES 68	
	15. SECURITY CLASS (of this report) UNCLASSIFIED	
15a. DECLASSIFICATION DOWNGRADING SCHEDULE		
16. DISTRIBUTION STATEMENT (of this Report) Approved for public release; distribution unlimited.		
17. DISTRIBUTION STATEMENT (of the abstract entered in Block 20, if different from Report)		
18. SUPPLEMENTARY NOTES This work sponsored by the Defense Nuclear Agency under RDT&E RMSS Code B344078464 Y99QAXSC06157 H2590D.		
19. KEY WORDS (Continue on reverse side if necessary and identify by block number) Inelastic Soil-Structure Interaction Doubly-Asymptotic Approximations Boundary Element Techniques		
20. ABSTRACT (Continue on reverse side if necessary and identify by block number) This report describes a doubly-asymptotic (DA), boundary-element (BE) treatment of a surrounding nonlinear soil medium for dynamic soil- structure interaction analysis. Linear soil-structure interaction is reduced to a surface relationship that is asymptotically exact at both high and low frequencies. Nonlinear soil-structure interaction is treated similarly, except a volume contribution is added in the volume; a quasi- static and quasi-dynamic (axisymmetric) problem for which finite-element		

DD FORM 1473 1 JAN 73

EDITION OF 1 NOV 65 IS OBSOLETE

UNCLASSIFIED

SECURITY CLASSIFICATION OF THIS PAGE (When Data Entered)

210 118

UNCLASSIFIED

SECURITY CLASSIFICATION OF THIS PAGE(When Data Entered)

20. ABSTRACT (Continued)

solutions have been obtained for comparison. For soil behavior based on J_2 -plasticity theory, reasonable agreement is obtained. For soil behavior based on the Cap model, which is a combined I_1 - and J_2 -plasticity theory agreement is not obtained.

UNCLASSIFIED

SECURITY CLASSIFICATION OF THIS PAGE(When Data Entered)

PREFACE

The authors express their appreciation to Drs. C. A. Felippa and K. C. Park for valuable consultation on the intricacies of nonlinear boundary integral equations and their numerical solution. In addition Drs. H. Levine and S. Pang of Weidlinger Associates, Menlo Park, CA, provided valuable consultation on soil-structure interaction, the Cap model, and provided the TRANAL check results. A debt is also owed to Dr. C.-L. Yen for providing important analytical check results and Dr. R. Murtha, NCL, for providing the NONSAP check results.

ACCESSION for		
NTIS	White Section	<input checked="" type="checkbox"/>
DDC	Buff Section	<input type="checkbox"/>
UNANNOUNCED		<input type="checkbox"/>
JUSTIFICATION		
BY		
DISTRIBUTION/AVAILABILITY CODES		
Dist.	AVAIL and/or	SPECIAL
A		

TABLE OF CONTENTS

<u>Section</u>	<u>Page</u>
I INTRODUCTION - - - - -	5
II TECHNICAL DISCUSSION - - - - -	7
2.1 REVIEW OF THE LINEAR DAA FORMULATION - - - - -	7
2.2 NONLINEAR DAA FORMULATION - - - - -	8
2.2.1 Quasi-Static DAA - - - - -	10
2.2.2 Quasi-Dynamic DAA - - - - -	13
2.3 ALTERNATE FORMULATIONS - - - - -	15
2.3.1 Body Force Formulation - - - - -	16
2.3.2 Infinite Elements - - - - -	17
2.3.3 Separation Model - - - - -	17
2.4 COMPUTATIONAL STRATEGY - - - - -	18
2.4.1 Overview of Nonlinear Computations - - - - -	18
2.4.2 Volume Information Computations - - - - -	19
III NUMERICAL RESULTS - - - - -	27
3.1 ELASTIC MEDIUM: DAA AND EXACT RESULTS - - - - -	28
3.2 ELASTIC MEDIUM: DAA, BODY-FORCE AND EXACT RESULTS - - - - -	28
3.3 J_2 -THEORY MEDIUM: DAA AND NONSAP RESULTS - - - - -	29
3.4 CAP-MODEL MEDIUM: QUASI-STATIC DAA AND TRANAL RESULTS - - - - -	30
3.5 CAP-MODEL MEDIUM: QUASI-DYNAMIC DAA AND TRANAL RESULTS - - - - -	31
3.6 CAP-MODEL MEDIUM: BODY-FORCE RESULTS - - - - -	32
IV CONCLUSION - - - - -	46
REFERENCES - - - - -	47

Appendices

A WAVE DECOUPLING APPROXIMATION - - - - -	A-1
B OUTLINE OF THE DERIVATION OF THE BOUNDARY INTEGRAL EQUATION FOR INELASTIC MEDIUM - - - - -	B-1
C NUMERICAL EVALUATION OF NONLINEAR COEFFICIENT MATRICES - - - - -	C-1
D BOUNDARY INTEGRAL EQUATION MATRICES WITH SYMMETRY CONDITIONS - - - - -	D-1

LIST OF ILLUSTRATIONS

<u>Figure</u>		<u>Page</u>
1	Displacement characteristics - - - - -	23
2	Plastic strain increments - - - - -	24
3	Quadrature elements - - - - -	25
4	Snapshot of medium displacement (quasi-dynamic model) - - - - -	26
5	Elastic response: DAA and exact - - - - -	33
6	Elastic response: body force damping and exact - - - - -	34
7	Elastic plastic J_2 cavity response - - - - -	35
8	Elastic plastic Cap model response, short pulse - - - - -	36
9	Elastic plastic Cap model response, long pulse - - - - -	37
10	Elastic plastic Cap model response, short pulse, and with "separation" - - - - -	38
11	Elastic plastic Cap model response, long pulse, and with "separation" - - - - -	39
12	Elastic plastic Cap model response, short pulse, and body force damping - - - - -	40
13	Elastic plastic Cap model response, short pulse, body force damping, and with "separation" - - - - -	41
A-1	1-D quasi-static problem - - - - -	A-3
C-1	Area integration element definition - - - - -	C-3
C-2	Geometry for cases 2 and 3 - - - - -	C-4
D-1	Axis of symmetry - example problem - - - - -	D-3

LIST OF TABLES

<u>Table</u>		<u>Page</u>
1	DAA-SSI check runs: 1 - - - - -	42
2	Material properties - - - - -	43
3	DAA-SSI check runs: 2 - - - - -	44
4	Material properties - - - - -	45

SECTION I
INTRODUCTION

The treatment of soil-structure interaction is of considerable importance in analyses of the integrity of structures in ground-shock environments. There is currently one basic approach to the nonlinear treatment of the problem: finite element or finite difference methods. Finite element or finite difference methods can model the problem to almost any accuracy desired but the large number of equations required generally precludes efficient computation. The number of equations can be reduced through special elements representing quiet boundaries or specific radiation properties, but modeling with these special elements requires considerable skill and may necessitate a complete finite element model for validation. An approach to achieve a method more versatile than special elements and more economical than finite element or finite difference for the treatment of these problems may be to consider a boundary element formulation. Such an approach is pursued in this study: an analytical approximation of the soil-structure interaction requiring boundary elements is combined with the modeling capabilities of the finite element (FE) method while avoiding the burden of many elements in the soil.

This report examines a boundary-element (BE) treatment of the surrounding nonlinear soil that is an extension of a BE method for a linear soil [1]. In the linear problem, the structure was modeled with an available FE code, and the soil-structure interaction was reduced to a surface relationship through the use of a doubly asymptotic approximation (DAA) [2], which required the application of BE techniques [3]. The linear study focused on the two-dimensional plane-strain response of structures surrounded by an infinite elastic medium; the approach was shown to produce results of acceptable accuracy.

In the nonlinear soil problem, the linear structure is still modeled with an available FE code. The soil-structure interaction is reduced to a surface relationship for the linear portion of the soil behavior and a volume relationship for the nonlinear portion through the use of a modified DAA, which still involves the application of BE techniques. The nonlinear problem requires a considerable increase in the complexity of the analysis. One, volume information is needed to evaluate the volume relationship; hence, additional data must be generated and stored. Two, the DAA must be modified to provide a wave propagation model for soil response based on an I_1 -plasticity model. And three, the wave-decoupling that occurs from assuming the incident and scattered waves are algebraically additive must be examined carefully.

To study the nonlinear problem effectively, a simple problem that retains the physics but eliminates much of the generality was developed. The simple problem is the axisymmetric response of an internally loaded, plane strain circular infinite shell surrounded by an infinite 2-D nonlinear soil. This model eliminates the wave-decoupling, since there is no incident wave, but includes the first two aspects of the nonlinear problem. A simple study of the wave-decoupling effect, not considered in this report, is given in Appendix A.

The report first addresses the outline of the theory: the linear theory is reviewed, the governing nonlinear equations are given, and alternate approaches are considered. Then the computational strategy is presented, followed by numerical results and conclusions. Figures and tables are grouped at the end of the section in which they are first mentioned.

SECTION II

TECHNICAL DISCUSSION

The first part of this section describes the theoretical development of doubly asymptotic, boundary-integral analysis techniques for nonlinear media. First, the elastic formulation is reviewed [1, 2]. Then the extension to inelastic soil response is described. The introduction of the doubly asymptotic approximation leads to two possible formulations for the treatment of inelastic effects; both of these are considered. In addition, two alternate formulations are presented.

Treatment of an inelastic material by the boundary element method has been described in considerable detail by Swedlow and Cruse [3] and by Mendelson [4]. Mukerjee [5], however, has shown that these descriptions are incorrect for two-dimensional plane-strain response. The results of these previous developments are used in this report without detailed derivation; however, an outline of the correct derivation is given in Appendix B.

The second part of this section describes the computational strategy used to solve the equations governing inelastic soil-structure interaction. Emphasis is placed on the methods used to determine the volume information, displacements, strains and nonlinear effects. The details of the linear portion of the computations have been treated previously [1].

2.1 REVIEW OF THE LINEAR DAA FORMULATION

The matrix FE equation of motion for a linear-elastic structure, embedded in a surrounding linear-elastic medium and excited by known forces applied to the structure and by an incident wave propagating through the medium, is

$$\underline{\underline{M}}_s \ddot{\underline{q}} + \underline{\underline{K}}_s \underline{q} = \underline{f}_s + \underline{f}_I + \underline{f}_S \quad (1)$$

where $\underline{\underline{M}}_s$ and $\underline{\underline{K}}_s$ are the mass and stiffness matrices for the structure, \underline{q} is the structural displacement vector, \underline{f}_s is a vector of known forces applied to the structure, \underline{f}_I and \underline{f}_S are surface-force vectors associated with the incident and scattered waves, respectively, and a dot denotes temporal differentiation. The DAA is now introduced to evaluate the scattered force vector \underline{f}_S [2]. This approximation, which is a surface interaction approximation that replaces the infinite volume of an external surface of the structure, is expressed as [1]

$$\underline{f}_S = \rho \underline{D}^T \underline{G}^T \underline{A} \underline{C}_m \underline{G} \dot{\underline{u}}_S + \underline{D}^T \underline{K}_m \underline{u}_S \quad (2)$$

where ρ is the mass density of the medium, \underline{D} and \underline{G} are coordinate transformation matrices, \underline{A} is a diagonal surface element area matrix, \underline{C}_m is a diagonal sound-speed matrix for the medium, \underline{K}_m is a full surface-stiffness matrix for the medium, \underline{u}_S is the computational scattered-displacement vector for the surface elements, and a superscript T denotes matrix transposition. The doubly asymptotic nature of the DAA is apparent from (2), i.e., at low frequencies, $\dot{\underline{u}}_S$ is small relative to \underline{u}_S , and (2) reduces to a static stiffness relation; at high frequencies, the reverse is true, and (2) reduces to a radiation damping relation.

With structure-medium surface compatibility and elastic field superposition requiring that $\underline{D}\underline{q} = \underline{u}_I + \underline{u}_S$, (1) and (2) may be combined to obtain

$$\underline{M}_S \ddot{\underline{q}} + \rho \underline{D}^T \underline{A} \underline{C}_m \underline{G} \underline{D} \dot{\underline{q}} + (\underline{K}_S + \underline{D}^T \underline{K}_m \underline{D}) \underline{q} = \underline{f}_S + \underline{f}_I + \rho \underline{D}^T \underline{G}^T \underline{A} \underline{C}_m \underline{G} \dot{\underline{u}}_I + \underline{D}^T \underline{K}_m \underline{u}_I. \quad (3)$$

In the development of the nonlinear problem that follows, only known forces applied to the structure are considered, so $\underline{f}_I = \underline{u}_I = \underline{0}$. For this situation, (3) reduces to

$$\underline{M}_S \ddot{\underline{q}} + \rho \underline{D}^T \underline{G}^T \underline{A} \underline{C}_m \underline{G} \underline{D} \dot{\underline{q}} + (\underline{K}_S + \underline{D}^T \underline{K}_m \underline{D}) \underline{q} = \underline{f}_S \quad (4)$$

2.2 NONLINEAR DAA FORMULATION

In (4), the elements of \underline{C}_m are the dilatational and shear sound speeds for the medium [1]. One effect of inelastic behavior is to alter these sound speeds; at present, however, this alteration is neglected on the assumption that the dominant effect of inelastic behavior of the medium manifests itself in a displacement-dependent form. Also note that the assumptions ($\underline{u} = \underline{u}_I + \underline{u}_S$ and $\underline{f} = \underline{f}_I + \underline{f}_S$) alter the functional dependence of the incident and scattered waves, an important consideration for the nonlinear problem. A simple study of these assumptions are presented in Appendix A, but the effects of the assumptions are not considered further in this report.

In order to include the displacement-dependent effects of material inelasticity, it is necessary to consider the two-dimensional boundary-integral equation [3,4,5]

$$\lambda u^k(P) + \int_L T^{kl}(P,Q) u^l(Q) dL(Q) = \int_L U^{kl}(P,Q) t^l(Q) dL(Q) + \int_A \Sigma^{lmk}(p,Q) \epsilon_p^{lm}(p) dA(p) - \int_A U^{kl}(p,Q) b^l(p) dA(p) \quad (5)$$

where P is a point either on the structure-medium interface L or in the surrounding region A, Q is a point on L, p is a point in A, $\lambda = \frac{1}{2}$ if P is on L and $\lambda = 1$ if P is in A, u^k and t^k are components of the displacement and traction vectors pertaining to the k th Cartesian direction, respectively, $T^{k\ell}$ and $U^{k\ell}$ are components of second-order tensors, which constitute Green's functions, $\Sigma^{\ell mk}$ is a component of a third-order tensor, which also constitutes a Green's function, $\epsilon_p^{\ell m}$ is a component of the plastic-strain tensor and b^ℓ is a component of a body force vector in A. Through the division of L into a series of boundary elements (BE), and A into an array of finite quadrature elements (QE), (5) may be expressed in matrix notation, for \underline{u} and \underline{t} on L, as

$$\underline{S}\underline{u} = \underline{F}\underline{t} + \underline{B}\underline{\epsilon}_p - \underline{E}\underline{b} \quad (6)$$

in which the 2x2 elements of S, F and E are given by

$$\begin{aligned} S_{ij}^{k\ell} &= \frac{1}{2}\delta_{ij}\delta_{k\ell} + \int_{L_j} T_{ij}^{k\ell} \xi_j^\ell dL_j \\ F_{ij}^{k\ell} &= \int_{L_j} U_{ij}^{k\ell} \eta_j^\ell dL_j \\ E_{ij}^{k\ell} &= \int_{A_j} U_{ij}^{k\ell} \psi_j^\ell dA_j \end{aligned} \quad (7)$$

and the 2x3 elements of B are given by

$$B_{ij}^{\ell mk} = \int_{A_j} \Sigma_{ij}^{\ell mk} \eta_j^{\ell m} dA_j \quad (8)$$

In (6) $\underline{\epsilon}_p$ is arranged in groups as $(\epsilon_p^{11}, \epsilon_p^{12}, \epsilon_p^{22})_j$ and \underline{b} as (b^{11}, b^{22}) . In (7), δ_{ij} and $\delta_{k\ell}$ are Kronecker deltas, i and j are BE indices for L in the first two of (7), j is a QE index for A in the third of (7), ξ_j^ℓ and η_j^ℓ are assumed BE shape-functions, ψ_j^ℓ is an assumed QE shape-function, L_j is the length of the j th boundary element, and the kernels $T_{ij}^{k\ell}$ and $U_{ij}^{k\ell}$ are given in Appendix B. In (8), i is a BE index for L, j is a QE index for A, $\eta_j^{\ell m}$ is an assumed QE shape-function, A_j is the area of the j th QE, and the kernel $\Sigma_{ij}^{\ell mk}$ is given in Appendix B.

In the present implementation, the shape functions ξ_j^ℓ , η_j^ℓ , ψ_j^ℓ , and $\eta_j^{\ell m}$ are taken as unity over each element, so that each element is described by a single, centrally located, nodal point. Hence, $U_{ij}^{k\ell}$ constitutes the displacement in the k th

direction at nodal point i due to a unit point load in the ℓ th direction at a point on element j . The associated stresses at i are given by $\sigma_{ij} = \sum_{\ell mk} \sigma_{ij}^{\ell mk} e_k$, where the e_k are the Cartesian base vectors. Incidentally, $T_{ij}^{k\ell} = \sum_{\ell mk} n_i^k n_j^m$, where the n_i^k are the direction cosines for the surface normal at i . The numerical integration method used to evaluate the first two of (7) is described in [1], and the method used for the last of (7) and for (8) is given in Appendix C.

In (6) \underline{F} is a nonsingular matrix; hence (6) may be rewritten as

$$\underline{t}_S = \underline{K}_m \underline{u}_S - \underline{F}^{-1} \underline{B} \underline{\varepsilon}_p + \underline{F}^{-1} \underline{E} \underline{b} \quad (9)$$

where $\underline{K}_m = \underline{F}^{-1} \underline{S}$ is the linear surface-stiffness matrix for the medium [see (2)] and the subscript S has been added to indicate that the scattered wave is modeled. Equations (2) and (9) are now combined to give

$$\underline{f}_S = \rho \underline{D}^T \underline{G}^T \underline{A} \underline{C}_m \underline{G} \dot{\underline{u}}_S + \underline{D}^T \underline{K}_m \underline{u}_S - \underline{D}^T \underline{F}^{-1} \underline{B} \underline{\varepsilon}_p + \underline{D}^T \underline{F}^{-1} \underline{E} \underline{b} \quad (10)$$

which represents a possible DAA for an inelastic medium. In the development that follows, the body force \underline{b} is not considered until the alternate formulations are presented; see Section 2.3. In 2.3.1 the body force is viewed as the acceleration of the medium and the linear damping term, the first term in (10), is replaced by the body force term. The requirements and assumptions used to derive (3) and (4) are applied again to combine (1) and (10) to obtain the governing nonlinear equation of motion

$$\underline{M}_S \ddot{\underline{q}} + \rho \underline{D}^T \underline{G}^T \underline{A} \underline{C}_m \underline{G} \underline{D} \dot{\underline{q}} + (\underline{K}_S + \underline{D}^T \underline{K}_m \underline{D}) \underline{q} = \underline{f}_S + \underline{Q} \quad (11)$$

where $\underline{Q} = \underline{D}^T \underline{F}^{-1} \underline{B} \underline{\varepsilon}_p$ is a psuedo-force vector that accounts for medium inelasticity. As the DAA is a surface approximation [1] and the evaluation of \underline{Q} requires volume information to calculate $\underline{\varepsilon}_p$, an additional model must be constructed to generate the volume information. Two possible volume-information models are now examined.

2.2.1 Quasi-Static DAA

Inasmuch as the psuedo-force vector \underline{Q} may be viewed as a correction to the linear surface-stiffness force-vector $\underline{D}^T \underline{K}_m \underline{D} \underline{q}$, a possible volume-information model might derive from the static solution for the medium based on the current soil-structure tractions and displacements. In [3,4,5] integral-equation formulas are given for medium strains due to boundary tractions and displacements; these may be cast into matrix notation for easy computational implementation. Unfortunately,

these strain formulas did not prove to be computationally efficient. The kernels were poorly behaved because they are based on derivatives of the U_{ij}^{kl} kernel, which itself exhibits marginal numerical behavior. This difficulty was overcome through the use of the boundary-integral equation for displacements due to boundary tractions and displacements, i.e., (5) with $\lambda = 1$. In matrix notation (5) becomes, for $\lambda = 1$,

$$\underline{u}_m = - \hat{S} \underline{u} + \hat{F} \underline{t} + \hat{B} \underline{\varepsilon}_p \quad (12)$$

where \underline{u}_m is the displacement vector in the medium, \underline{u} and \underline{t} are the boundary-displacement and boundary-traction vectors, the 2x2 elements of \hat{S} and \hat{F} are given by

$$\begin{aligned} \hat{S}_{ij}^{kl} &= \int_{L_j} T_{ij}^{kl} \xi_j^\ell dL_j \\ \hat{F}_{ij}^{kl} &= \int_{L_j} U_{ij}^{kl} \eta_j^\ell dL_j \end{aligned} \quad (13)$$

and the 2x3 elements of \hat{B} are given by

$$\hat{B}_{ij}^{\ell mk} = \int_{A_j} \Sigma_{ij}^{\ell mk} \eta_j^{\ell m} dA_j \quad (14)$$

Most of the symbols in (12), (13), and (14) have been defined previously; here, however, i is a QE index for A and j is a BE index for L in (13), and i and j are QE indices for A in (14).

Equation (12) efficiently provides the displacements in the medium; from these displacements, the strains are quickly computed from finite-difference expressions. With the strains available, the computations to determine $\underline{\varepsilon}_p$ from the inelastic medium behavior proceed in a straightforward manner; the details are given in Section 2.4.

A difficulty was encountered in using the quasi-static DAA formulation for one of the two inelastic soil models considered. To explain this difficulty, it is necessary to discuss briefly the two inelastic soil models.

The first model considered, the mechanical sublayer model [6], is a basic J_2 (second deviatoric stress-tensor invariant) flow rule theory commonly used for the elasto-

plastic behavior of metals. This model was chosen because it is simple and because a computational subroutine was readily available at the laboratory. It was recognized that this model would not properly represent soil behavior but it would provide a first step in the verification of the nonlinear DAA formulation. As shown in Section 3.0, the quasi-static DAA with this plasticity model produced acceptable results.

The second model considered is a cap model [7], herein called the Cap model (also see [8] for details of the Cap model subroutine). This inelastic soil model was developed to model granular soils under dynamic loading conditions and is based on a yield (failure) surface that is a function of I_1 (first stress-tensor invariant) and J_2 . Although this model is regarded as an excellent model for dynamically loaded soils, it appears to be incompatible with the static soil behavior assumed for the quasi-static DAA formulation.

To understand the difficulty encountered with the Cap model, the static solution of the 2-D plane strain cylindrical cavity of radius a for internal loading in an infinite elastic medium is considered. For an internal axisymmetric applied displacement, u_a , or a pressure giving rise to u_a , the displacement and stresses in the elastic medium are

$$u_r = \frac{u_a a}{r}, \quad u_\theta = 0 \quad (15)$$

and

$$\sigma_r = \frac{2u_a aG}{r^2} = -\sigma_\theta; \quad \sigma_z = 0 \quad (16)$$

where u_r and u_θ are the radial and tangential displacements, r is the radial coordinate measure, σ_r , σ_θ and σ_z are the stresses in cylindrical coordinates and G is the elastic shear modulus. With this stress field (16), the expression for I_1 becomes

$$I_1 \equiv \sigma_r + \sigma_\theta + \sigma_z = 0 \quad (17)$$

Hence, for this simple axisymmetric static problem, I_1 is always zero, and the quasi-static DAA formulation produces a stress field with no I_1 component. In the actual dynamic problem, inertial forces in the medium give rise to a significant I_1 component, as well as a J_2 component, so that the stress state at the failure surface is quite different from that predicted by the quasi-static DAA. Hence, the quasi-static DAA formulation does not produce responses that are comparable to a finite-element dynamic response calculation.

In summary, although the result for the quasi-static DAA with a J_2 plasticity model were encouraging, the results with the Cap model were not. Therefore a DAA formulation that more realistically reflects the dynamic nature of the problem was explored.

2.2.2 Quasi-Dynamic DAA

As the DAA was known to produce good results for an elastic problem, the physical model that corresponds to the elastic DAA was sought. This development can most easily be described in terms of the following problem: the plane-strain excitation of an infinite medium surrounding an infinite, circular cylindrical cavity by means of transient pressurization of the cavity.

For a linear medium, the DAA says that radial stress is given by

$$\sigma_r(r,t) = -\rho c_\phi \dot{u}_r(r,t) - \frac{2\mu}{r} u_r(r,t) \quad (18)$$

where the DAA surface (i.e., the surface defined by the soil-structure interface) has been positioned at an arbitrary radial position r . In this equation, ρ , c_ϕ and μ are the density, dilatational velocity and shear modulus for the medium, respectively, u_r is radial displacement, and the dot denotes temporal differentiation. But, from elasticity theory,

$$\begin{aligned} \sigma_r(r,t) &= \rho \ddot{\phi} - \frac{2\mu}{r} u_r(r,t) \\ u_r(r,t) &= \frac{\partial}{\partial r} \phi(r,t) \end{aligned} \quad (19)$$

where ϕ is the dilatational displacement potential. Hence (18) and (19) yield, for the "internal forcing" problem considered here,

$$\phi(r,t) = \phi\left(a, t - \frac{r-a}{c_\phi}\right) \quad (20)$$

where a is the radius of the cavity. Now this result constitutes a plane-wave treatment of the radiated wave. Hence the DAA not only provides, through (18), a radiated-wave stress-displacement relation at $r = a$, but also provides the displacement field in the medium, viz.,

$$u_r(r,t) = u_r\left(a, t - \frac{r-a}{c_\phi}\right) \quad (21)$$

For an elasto-plastic medium, a surface relation such as (18) is not sufficient to determine surface response. In this case, "volume information" is also needed.

Such information is provided by application of the method of characteristics to the radiated wave, which leads to the behavior illustrated in Figure 1. The characteristics, which constitute loci of constant displacement, define the displacement field in the medium at any time of interest. Straight characteristics indicate linear wave propagation, while curved characteristics indicate nonlinear wave propagation.

In accordance with Figure 1, nonlinear DAA computations proceed as follows:

1. Surface response is determined at $t = \Delta t$ based on linear-elastic medium behavior.
2. The surface displacement $u_r(a,0)$ is prescribed at $r - a = c_\phi \Delta t$ and average strains are calculated for the region $0 \leq r - a \leq c_\phi \Delta t$.
3. The state of the medium at $r = \Delta t$ is found to be linear-elastic.
4. Surface response is determined at $t = 2\Delta t$ based on linear-elastic medium behavior.
5. $u_r(a,0)$ and $u_r(a,\Delta t)$ are prescribed at $r - a = 2c_\phi \Delta t$ and $r - a = c_\phi \Delta t$, respectively; average strains are calculated for the region $0 \leq r - a \leq 2c_\phi \Delta t$.
6. The state of the medium at $t = 2\Delta t$ is found to be linear-elastic for $r - a \geq c_\phi \Delta t$ and inelastic for $r - a < c_\phi \Delta t$.
7. A local propagation velocity $c_2' = c(r=a)$ is calculated and surface response is determined at $t = 3\Delta t$ based on inelastic medium behavior.
8. $u_r(a,0)$, $u_r(a,\Delta t)$ and $u_r(a,2\Delta t)$ are prescribed at $r - a = 3c_\phi \Delta t$, $r - a = 2c_\phi \Delta t$ and $r - a = c_\phi \Delta t$, respectively; average strains are calculated for the region $0 \leq r - a \leq 3c_\phi \Delta t$.
9. The state of the medium at $t = 3\Delta t$ is found to be linear-elastic for $r - a \geq 2c_\phi \Delta t$ and inelastic for $r - a < 2c_\phi \Delta t$.
10. Local propagation velocities $c_3' = c(r=a)$ and $c_3'' = c(r=a+c_2'\Delta t)$ are calculated and surface response is determined at $t = 4\Delta t$ based on inelastic medium behavior.

Note that this procedure, which pertains to a volume-wave (VW) model, defines a new characteristics grid at each time step. For computational purposes, two single-dimension arrays are required to store the displacement and its radial location; for a nonaxisymmetric problem these would be two-dimensional arrays. Also in the calculations, characteristics-grid displacements and slopes (first-derivatives) are

interpolated to yield nodal values for a fixed spatial grid, from which medium strains are calculated. This is required for efficient computation of the volume integral for nonlinear DAA analysis; otherwise the boundary matrix \underline{B} [see (12)] would have to be recomputed at each time step. Note the volume matrices $\underline{\hat{S}}$, $\underline{\hat{F}}$ and $\underline{\hat{B}}$ in (12) are not required, so considerably less storage is required.

For the volume-wave model just discussed, radial displacement does not attenuate with distance [see (21)]. However, during the study of an alternate formulation, as discussed in Section 2.3, an attenuation of $\frac{1}{\sqrt{r}}$ was found to represent more accurately the exact response (as might be expected). Hence this attenuation was actually used to generate the characteristics-grid displacements for the VW model.

The quasi-dynamic DAA was partially successful. The no- I_1 problem encountered with the quasi-static DAA was not encountered with the quasi-dynamic formulation. The characteristics-grid displacements, described above, agree with FE solutions for very early times. At later times, however, agreement fades, because the tensile-cutoff feature in the Cap model produces displacement responses in the medium that are not properly treated by the simple characteristics method developed for the quasi-dynamic DAA. As partial compensation, the DAA characteristics-grid was modified to treat tensile cutoff (a loss of soil strength in tension) by not allowing a displacement to propagate into or out of a region of tensile cutoff. The displacement in the tensile cutoff region was interpolated from the two points adjacent to the region. This means that back reflections from the inner surface or a region in cutoff are ignored. Such reflections would be difficult to include in the calculations and would border on actually solving for the dynamic displacement field in the medium. The goal of this study has been to avoid costly calculations; the inclusion of reflections would be costly.

2.3 ALTERNATE FORMULATIONS

Two alternate formulations of the dynamic soil-structure interaction problem and a modification of the DAA approach are considered here. The first formulation treats the radiation damping in terms of a body-force field associated with the acceleration field in the medium, which is obtained from the volume-wave model discussed in Section 2.2.2. The second formulation is based on the use of "infinite elements" [10] in lieu of boundary elements. Finally, the DAA modification addresses tensile cutoff in the Cap plasticity model.

2.3.1 Body Force Formulation

This formulation is best explained by examining the governing equation for the medium and then reconsidering the arguments put forward to develop the DAA [1,2]. For two-dimensional plane strain, including plastic flow, the Navier equation, which governs the behavior of the medium, may be written as

$$\nabla^2 u_i + \frac{1}{1-2\nu}(u_{j,j})_{,i} = 2\epsilon_{ij,j}^p + \frac{2\nu}{1-2\nu}(\epsilon_{k,k}^p)_i - \frac{b_i}{G} + \rho \ddot{u}_i, \\ i, j, k = 1, 2, \quad (22)$$

where ∇^2 is the Laplacian operator, u is the displacement field, ν is Poisson's ratio, G is the elastic shear modulus, ϵ^p is the plastic strain field, b is the body force field, ρ is the mass density and a superimposed dot indicates a time derivative; see Appendix B for a derivation of (22). Terms appearing in the DAA relation (10) are readily associated with terms in (22). First, the stiffness-force term involving \underline{K}_m is associated with the left side of (22); second, the plastic term $\underline{B} \underline{\epsilon}_p$ is associated with the ϵ^p terms in (22); finally, the damping force term involving \underline{C}_m is associated with the inertia term $\rho \ddot{u}_i$ in (22) (see, e.g., [9]).

Rigorously speaking, the inertia term is costly to compute, requiring a finite-element model of the medium for practical problems. However, the volume-wave model described in Subsection 2.2.2 directly provides the displacement history of the medium, so that the acceleration \ddot{u}_i may easily be computed from a three-point backward difference formula. The static boundary integral equation (5) does not admit an acceleration term, but inertial forces may easily be included by considering them as body forces. Hence, from (22), the body-force computational vector in (9) is given by

$$\underline{b} = -\rho G \ddot{\underline{u}} \quad (23)$$

so that the surface relationship is given by (10) with $\underline{C}_m = 0$ and \underline{b} is given by (23). Hence, for $\underline{f}_s = \underline{f}_I = 0$, (1) becomes

$$\underline{M}_s \ddot{\underline{q}} + (\underline{K}_s + \underline{D}^T \underline{K}_m \underline{D}) \underline{q} = \underline{f}_s + \underline{Q} - \underline{D}^T \underline{F}^{-1} \underline{E} \underline{b}. \quad (24)$$

Solutions obtained from (24) were quite satisfactory for elastic medium response, but not satisfactory for inelastic response. To obtain converged solutions, the medium quadrature grid must be uniform and fixed-increment time integration is required. Even then, the medium solution jumps about too much to obtain smooth inelastic response.

2.3.2 Infinite Elements

In this section, some recent developments in the application of finite-element methods to infinite media are discussed [10]. Although an alternate formulation based on infinite elements was not pursued in this study, the formulation merits consideration, as it is attractive from two viewpoints [11]. First, the method is based on variational principles that provide symmetric matrices without resort to ad hoc symmetry procedures. Second, the extensive software developed for finite-element methods is directly applicable to these infinite elements. The second item is probably the more important, as a considerable portion of this study effort was devoted to the development of special software for boundary-integral equation methods. To date, infinite-element concepts have been applied only to fluid media [10], so further development work would be required for application to inelastic solid media.

2.3.3 Separation Model

One additional modeling concept was employed in an attempt to account more realistically for tensile cutoff phenomena embodied in the Cap plasticity model [7,8]. For the axisymmetric problems studied here, tensile cutoff occurs on a circle specified by a certain radial distance out from the soil-structure interface. As tensile cutoff represents the inability of the soil to support a tensile load, the soil beyond the tensile cutoff circle no longer provides stiffness and separation occurs. Hence, after tensile cutoff occurs, the system of interest is assumed to be composed of the structure and a surrounding annulus of soil, i.e., the soil is no longer infinite. This separation model can be partially, partially in that reflections from the tensile cutoff surface are not considered, incorporated in the computations. The incorporation involves a modification to the elastic soil contribution, the K_m matrix, and the inelastic contribution, Q . The procedures to affect the modifications are presented below, first for the elastic modification and then the inelastic one.

From the theory of elasticity [16], the stiffness for the infinite medium is

$$K_i = \frac{2\pi a p_i}{u_r(a)} = 4\pi G \quad (25)$$

and for the annulus

$$K_a = \frac{2\pi a p_i}{u_r(a)} = \frac{4\pi G (1+\nu) (b^2 - a^2)}{[(a^2 + b^2) + \nu(b^2 - a^2) - 2\nu^2 a^2]} \quad (26)$$

where p_i is the internal pressure, $u_r(a)$ is the radial displacement at the radius a where the pressure p_i is applied, G is the soil's shear modulus, ν is the soil's

Poisson's ratio, and b is the radius of the tensile cutoff circle. As a check, (26) reduces to (25) as $b \rightarrow \infty$. Hence the ratio of the two soil stiffnesses is obtained as

$$\kappa = K_a / K_i \quad (27)$$

and the separation due to tensile cutoff is accounted for by scaling \tilde{K}_m by κ to produce the correct stiffness for the annulus. The calculations for Q , the inelastic component, due to $\underline{\epsilon}_p$ are then performed for the annulus only. Note that the same model would be obtained if the soil matrices in (12) and (24) were recomputed for the proper annulus, but this would be very expensive. Unfortunately, the numerical results, Section 3.0, show that this additional "refinement" in the model did not greatly improve the results.

2.4 COMPUTATIONAL STRATEGY

The governing equations of motion for the DAA formulation (11) and for the body force formulation (24) are simply nonlinear second-order equations that are common in structural dynamics analysis. Therefore, these equations are readily solved by direct time integration methods for nonlinear structural dynamics analysis [12,13,14]. These methods fall into one of two categories: an implicit method [12] and an explicit method [13,14]; their relative merits will be discussed in Section 3. Both require that software be available to generate the linear coefficient matrices, the nonlinear terms and the forcing function. The procedures for the linear terms and the forcing function are presented in [1], so the emphasis here is on the nonlinear terms.

First, a brief overview of the steps required to compute the nonlinear terms is presented. Then the techniques used to implement the volume-wave model and the soil inelasticity treatment are discussed.

2.4.1 Overview of Nonlinear Computations

The plastic strain $\underline{\epsilon}^P$ is the key quantity that must be computed to solve the nonlinear equations (11) and (24). The medium acceleration is also needed for (24), but this is relatively simple to compute and will be dealt with later. The following steps are involved in the computation of $\underline{\epsilon}^P$:

1. At the n -th time step, the solution vector \underline{q}^n is known; hence, from $\underline{u}^n = \underline{Dq}^n$, \underline{u}^n is known.
2. The vector \underline{u}^n is used to compute the displacements in the medium, either from (12) or in accordance with the volume-wave model described in Subsection 2.2.2. The details of this calculation are considered below.

3. Through application of the proper differentiation formulas, the total-strain vector $\underline{\epsilon}^n$ is determined for the centroids of the quadrature elements in the medium. The details of this calculation are also considered below.
4. The strain-increment vector is determined from $\Delta \underline{\epsilon}^n = \underline{\epsilon}^n - \underline{\epsilon}^{n-1}$, where $\underline{\epsilon}^{n-1}$ has been retained from the previous time step.
5. The strain-increment vector $\Delta \underline{\epsilon}^n$ and the previous total-stress vector $\underline{\sigma}^{n-1}$ are sufficient to compute the total-stress vector at the n-th step, $\underline{\sigma}^n$, based on the inelastic constitutive relationships discussed in Subsection 2.2.1.
6. The elastic-strain vector $(\underline{\epsilon}^e)^n$ is computed as

$$(\underline{\epsilon}^e)^n = \underline{p}^{-1} \underline{\sigma}^n$$

where \underline{p} is the array of elastic-material coefficients that relates strains to stress.

7. The plastic-strain vector $(\underline{\epsilon}^p)^n$ is obtained as

$$(\underline{\epsilon}^p)^n = \underline{\epsilon}^n - (\underline{\epsilon}^e)^n$$

Figure 2 illustrates steps 6 and 7.

8. The nonlinear force \underline{Q}^n is computed by matrix-vector multiplication; see the definition following (11).
- 9a. For the explicit integrator, the solution at n+1 is obtained from information at n, so \underline{q}^{n+1} is now computed.
- 9b. For the implicit integrator, the solution at n+1 is obtained from an extrapolation based on \underline{Q}^n and \underline{Q}^{n-1} . The corrected value of \underline{Q}^{n+1} , which is computed from the solution \underline{q}^{n+1} is then compared to \underline{Q}^{n+1} - extrapolated; if the difference lies within an acceptable error bound, the integration proceeds; if not, an iteration procedure is carried out until satisfactory convergence is achieved within a reasonable number of iteration cycles or the calculation is aborted.

2.4.2 Volume Information Computations

The displacements in the medium are computed either from a quasi-static model, as described in Subsection 2.2.1, or from a quasi-dynamic model, as described in Subsection 2.2.2. The reason for computing the displacements in the medium is to determine strains by numerical differentiation. The plastic strains, assumed to be uniform

over each quadrature element, are computed at fixed grid points at the center of these prescribed quadrature elements. A sketch of some typical quadrature elements and the plastic strain points is shown in Figure 3.

For the quasi-static model the displacements in the medium are computed from (12), where the coefficient matrices are evaluated such that the displacements are obtained at the points marked with an x in Figure 3. These points are chosen to be half-way between the plastic strain points in both the radial and tangential directions. This location is ideal, as it avoids singular points in the evaluation of (12) and provides simple but accurate differentiation formulas to compute the strains. As an example, the strains at strain point 4 are computed as

$$\begin{aligned}
 \epsilon_r &= \frac{\partial u_r}{\partial r} = \frac{-u_r^5 + u_r^6}{\Delta r_{5-6}} \\
 \epsilon_\theta &= \frac{u_r}{r} + \frac{1}{r} \frac{\partial u_\theta}{\partial \theta} = \frac{u_r^5}{r^5} + \frac{u_r^6}{r^6} + \frac{2}{r^5 + r^6} \left(\frac{-u_\theta^8 + u_\theta^4}{\Delta \theta_{8-4}} \right) \\
 \gamma_{r\theta} &= \frac{1}{r} \frac{\partial u_r}{\partial \theta} + \frac{\partial u_\theta}{\partial r} - \frac{u_\theta}{r} \\
 &= \frac{2}{r^5 + r^6} \left(\frac{-u_r^8 + u_r^4}{\Delta \theta_{8-4}} \right) + \frac{-u_\theta^5 + u_\theta^6}{\Delta r_{5-6}} - \frac{u_\theta^5 + u_\theta^6}{r^5 + r^6}
 \end{aligned} \tag{28}$$

where the subscripts r, θ refer to the polar-coordinate directions and the superscripts refer to the medium displacement indices. Note that, for strain points adjacent to the boundary, e.g., 1,3,5, ... , the boundary-displacement value is used as one of the medium displacement points. In this study only calculations for axisymmetric problems were performed, so $\gamma_{r\theta}$ and the second term in ϵ_θ vanished. For general geometries, the quadrature elements may be viewed as finite elements, the medium displacements computed at the proper nodes, and standard finite-element methods used to compute the strain for the quadrature (finite) element [15].

For the quasi-dynamic model, the medium displacements are not computed at fixed points; instead, grid points are generated by the location of a particular displacement on its characteristic. These grid points are positioned as

$$\begin{aligned}
 d_1 &= \Delta t_1 \cdot c(d_1) + \Delta t_2 \cdot c(d_2) + \dots + \Delta t_n \cdot c(d_n) \\
 d_2 &= \Delta t_2 \cdot c(d_2) + \dots + \Delta t_n \cdot c(d_n) \\
 \vdots & \\
 d_n &= \Delta t_n \cdot c(d_n)
 \end{aligned} \tag{29}$$

where d_n is the radial distance from the boundary at time t_n , Δt_j is the j -th time step and $c(d_j)$ is the dilatational sound speed for the medium at the d_j location. The variation in the medium's sound speed is determined from

$$c = \sqrt{\frac{B + \frac{4}{3} \mu}{\rho}} \quad (30)$$

where B , the bulk modulus, and μ , the shear modulus, are determined from the stress and strain increments for the quadrature element under consideration.

As indicated in the displacement snapshot shown in Figure 4, the displacement of the medium at d_n is computed as

$$u_n = u(t_n) \sqrt{\frac{a}{a + d_n}} \quad (31)$$

where $u(t_n)$ is the radial displacement at the boundary at time t_n , and a is the radius of the boundary. This corresponds to cylindrical spreading of the scattered wave.

To compute strains, the slope $\partial u_r / \partial r$ and the displacement u_r are required at each plastic-strain point. These values are determined as follows. For plastic-strain point 1, the average slope and displacement over the quadrature element are computed as (see Figure 4)

$$\begin{aligned} \frac{\partial u_r}{\partial r}(P1) &= \frac{d_n}{\Delta R_1} \left(\frac{-u_{n+1} + u_n}{d_n} \right) + \frac{d_{n-1} - d_n}{\Delta R_1} \left(\frac{-u_n + u_{n-1}}{d_{n-1} - d_n} \right) \\ &+ \frac{\Delta R_1 - d_{n-1}}{\Delta R_1} \left(\frac{-u_{n-1} + u_n}{d_{n-2} - d_{n-1}} \right) \\ u_r(P1) &= \frac{d_n}{\Delta R_1} \left(\frac{u_{n+1} + u_n}{2} \right) + \frac{d_{n-1} - d_n}{\Delta R_1} \left(\frac{u_n + u_{n-1}}{2} \right) \\ &+ \frac{\Delta R_1 - d_{n-1}}{\Delta R_1} \left(\frac{u_{n-1} + u(\Delta R_1)}{2} \right) \end{aligned} \quad (32)$$

where $u(\Delta R_1)$ is evaluated at ΔR_1 by linear interpolation between u_{n-1} and u_{n-2} . For plastic-strain point 2 in Figure 4, the average slope is simply the slope of the straight line joining u_{n-1} and u_{n-2} , and the average displacement at the plastic-strain point is determined by linear interpolation between u_{n-1} and u_{n-2} .

After the strains are computed, Steps 4-9 in Subsection 2.4.1 are straightforward, as these steps are typical of any transient structural dynamics analysis,

[12,13,14,15]. Finally, the medium-acceleration values required in (23) are provided by numerical differentiation based upon displacement values at three consecutive time steps.

Note that displacements and strains are computed in polar coordinates [see, e.g., (32)], while the coefficient matrices for the governing equations (11) and (24) are computed in Cartesian coordinates, which are the global coordinates. Therefore, polar-coordinate displacements and strains are transformed to Cartesian coordinates before the matrix-vector multiplications in (11) or (24) are performed.

Because the nonlinear formulations require additional matrices, only one-half the problem is modeled to reduce storage requirements, with the x_2 -axis in Figure 3 chosen as a plane of symmetry. The symmetry condition is easily established for the FE structure [15], but that for the BE model is not as readily determined (see Appendix D). Finally, it is important to mention that, although calculations were only performed for axisymmetric problems, most of the analysis software was constructed to treat more general non-axisymmetric problems.

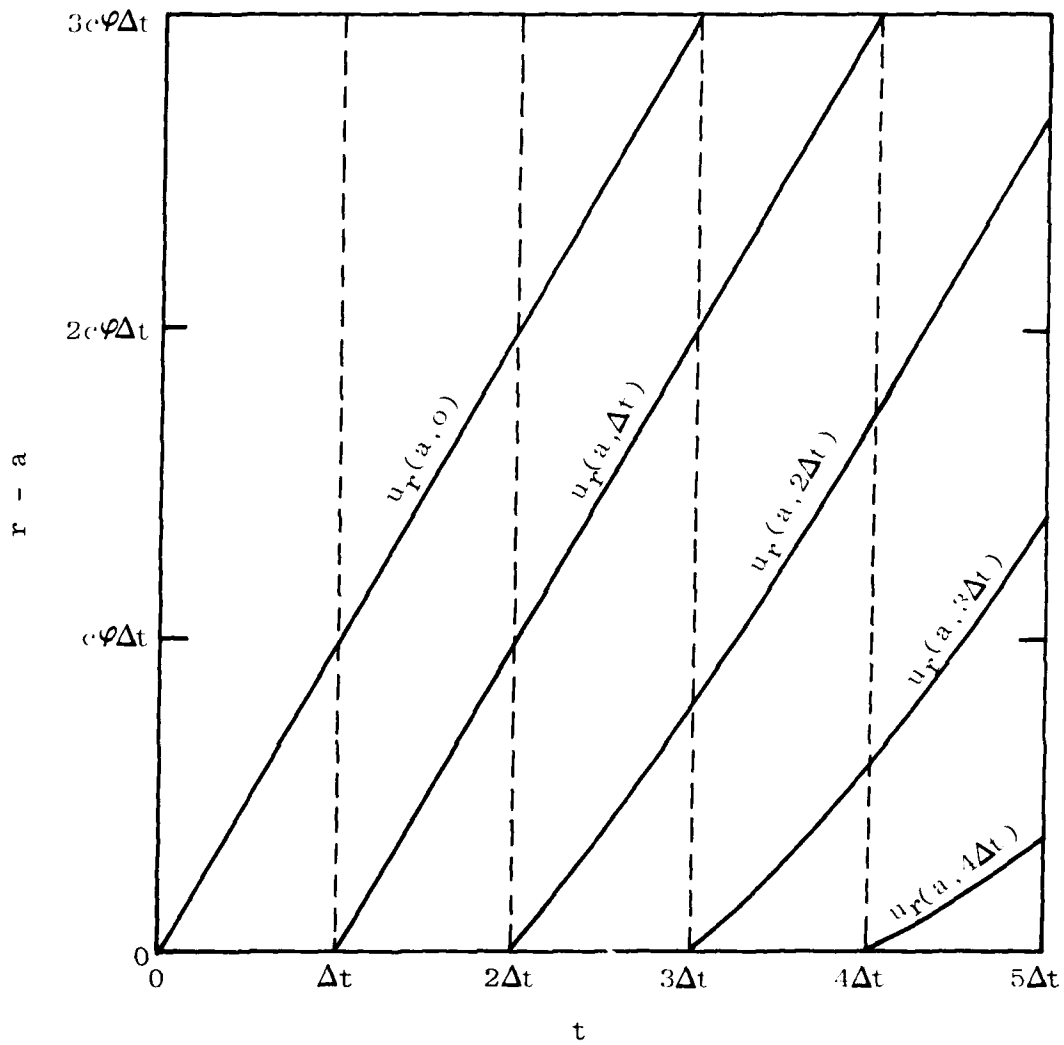


Figure 1. Displacement characteristics.

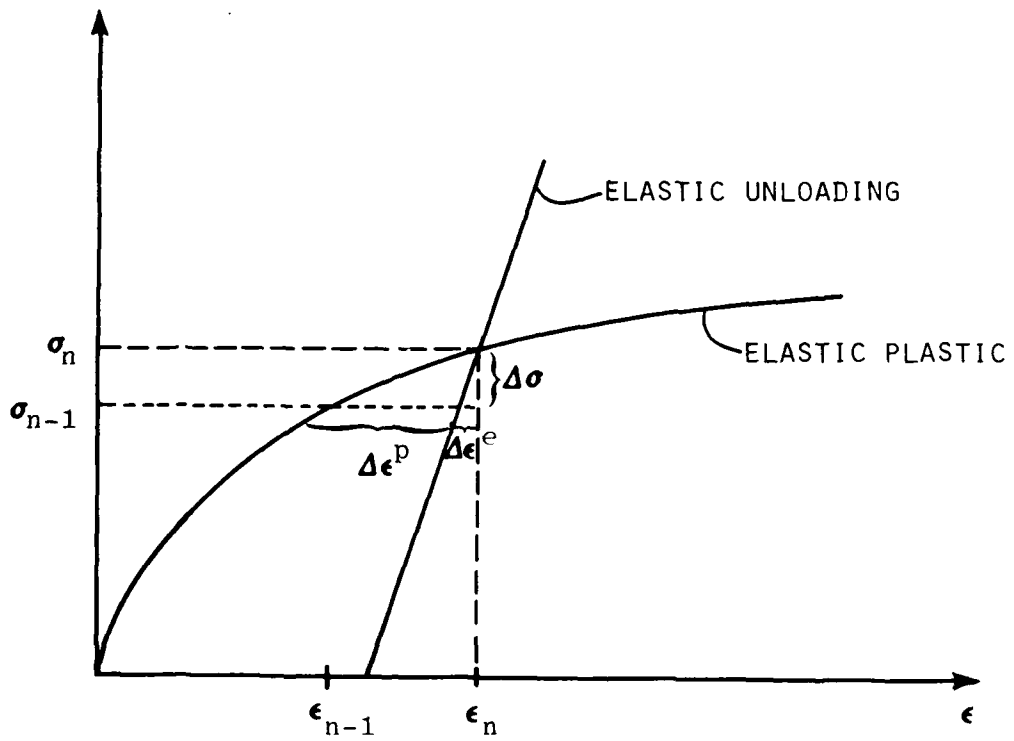
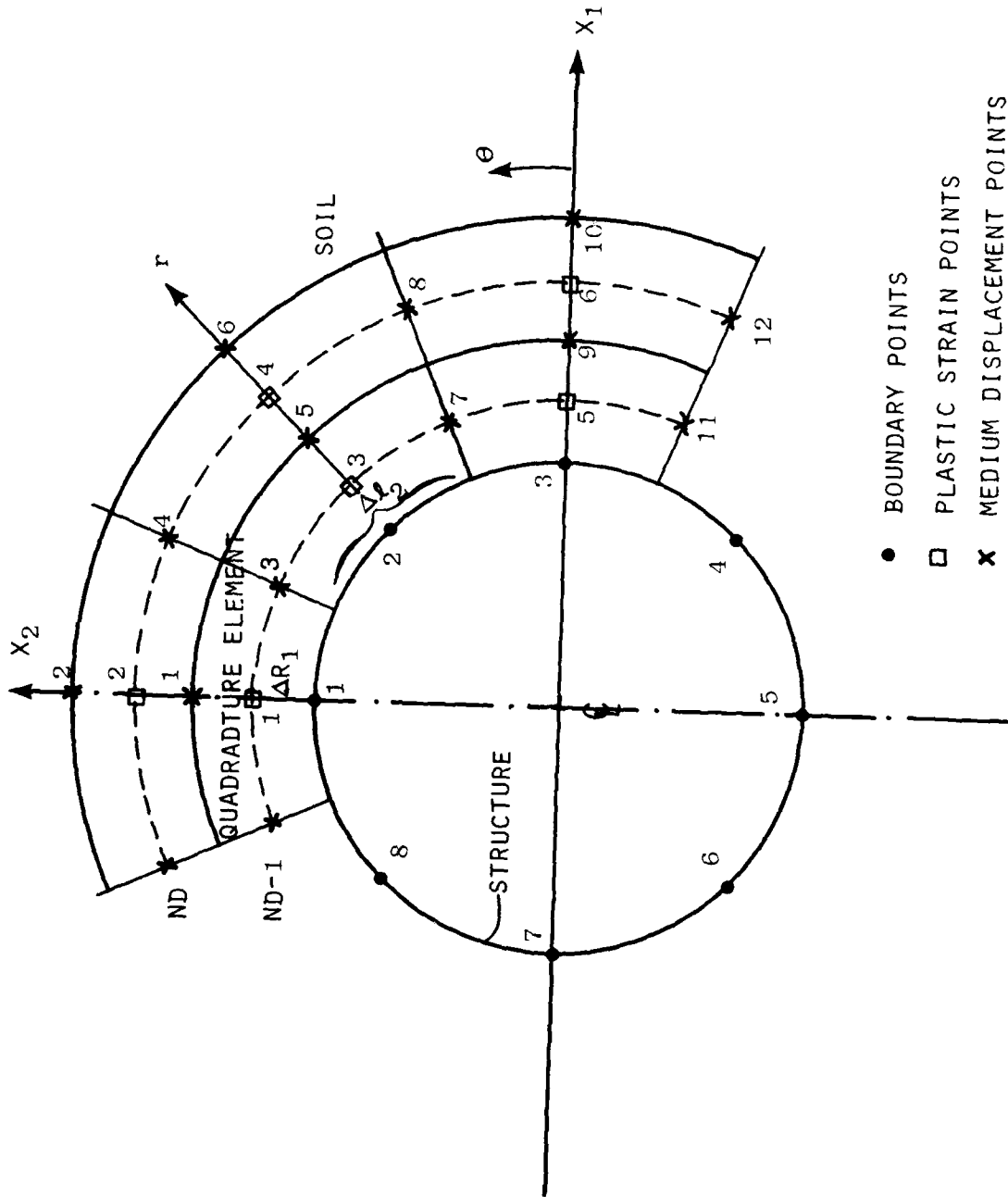


Figure 2. Plastic strain increments.



- BOUNDARY POINTS
- PLASTIC STRAIN POINTS
- x MEDIUM DISPLACEMENT POINTS

Figure 3. Quadrature elements.

SECTION III

NUMERICAL RESULTS

The numerical results presented in this section illustrate the characteristics of the soil-analysis formulations described in Section 2. All the results pertain to the axisymmetric response of either an infinite, circular cylindrical cavity or an infinite, circular cylindrical shell surrounded by an infinite soil-medium to an internal triangular pressure pulse. The computational model for the shell is a finite-element one, as provided by the REXBAT Code [17]. Two inelastic models for the soil are considered: 1) the J_2 mechanical sublayer model [6] and 2) the Cap model [7,8]; see Subsection 2.2.1. As eight elements over half the circumference (the x_2 -axis being the symmetry axis) produce excellent results for the elastic problem, eight elements are used in all the examples. The governing equations of motion are solved with the stand-alone time-integration packages described in [12, 13 and 14]. These packages permit both automatic-step and fixed-step integration using the implicit Park method [12] or the explicit central-difference method [13,14].

The following comparisons are presented in this section:

1. Responses produced by the doubly asymptotic approximation (DAA) are compared with exact responses for an elastic medium surrounding an infinite cylindrical cavity;
2. DAA and body-force responses are compared with exact responses for an elastic medium surrounding an infinite cylindrical shell;
3. Quasi-static and quasi-dynamic DAA responses are compared with NONSAP responses for an inelastic (J_2 -plasticity theory) medium surrounding an infinite cylindrical cavity;
4. Quasi-static DAA responses are compared with TRANAL responses for an inelastic (Cap model) medium surrounding an infinite cylindrical shell;
5. Quasi-dynamic DAA responses are compared with TRANAL responses for an inelastic (Cap model) medium surrounding an infinite cylindrical shell; and
6. Quasi-dynamic body-force responses are compared with TRANAL responses for an inelastic (Cap model) medium surrounding an infinite cylindrical shell.

The first three comparisons demonstrate the satisfactory accuracy of the DAA and body force formulations for an elastic medium, and a J_2 -plasticity model inelas-

tic medium. The remaining comparisons demonstrate the unsatisfactory accuracy of these formulations for the Cap model inelastic media.

3.1 ELASTIC MEDIUM: DAA AND EXACT RESULTS

In [1], the elastic response of an infinite cylindrical shell embedded in an elastic medium to an incident dilatational wave was computed with the DAA formulation and compared with the corresponding exact response. Satisfactory agreement was observed. In this study, internal triangular pressure pulses are considered in lieu of an incident wave. Hence, it is appropriate to compare results produced by the DAA formulation with their exact counterparts for the internal loading.

The problem considered is the response of a cavity in a 2-D plane strain elastic medium with an elastic shear modulus, G , of 200,000 psi, Poisson's ratio, ν , of 0.25 and a weight density of 117 lbs/ft³. The internal pressure pulse is an isosceles triangle of durations τ , 2τ , 4τ and 8τ , where τ is the transit time of a dilatational wave across the diameter of the cavity. The exact response is obtained by the residual potential method [2] and the DAA response is obtained by discrete element methods [1]. The DAA peak-displacement errors are 20.8%, 24.1%, 22.7% and 15.7% for the pulse widths of τ , 2τ , 4τ and 8τ , respectively. These DAA results are not as accurate as those reported in [1], but they are still considered acceptable; the introduction of a cylindrical shell would yield results accurate to within 10%-20%, as observed in [1]. Note that the most inaccurate responses are obtained for the intermediate pulses, whose dominant frequency components lie in the intermediate frequency range, where the DAA is most inaccurate.

3.2 ELASTIC MEDIUM: DAA, BODY-FORCE AND EXACT RESULTS

This problem was studied to determine the proper volume-wave model (Subsection 2.2.2) and to illustrate the accuracy of the body-force formulation (Subsection 2.3.1). The problem models the response of an infinite cylindrical shell of radius/thickness = 50, where the radius is 1m (39.3701 in.), $E = 30 \times 10^6$ psi, $\nu = 0.3$, and $\rho = 460$ lb/ft³ embedded in an elastic soil which has the following properties: $G = 559$ ksi, $\nu = 0.3313$, and $\rho = 125$ lb/ft³. The pressure pulse is a triangle with a rise time of 0.07288 ms, a duration of 0.7288 msec (1 transit time across the diameter) and a peak pressure of 1 ksi.

Figure 5 shows exact [2] and DAA [see equation (4)] displacement responses. Note that the DAA underpredicts the peak and is more heavily damped. Figure 6 illustrates the displacement responses for the exact and body-force, (25) with $\underline{Q} = \underline{Q}$, formulations. Note that the peaks are nearly identical; the only difference occurs at

later times. The difference occurs because the body-force calculation is very sensitive to numerical noise that accumulates throughout the computations. To achieve the results shown in Figure 6 the characteristics volume-wave model displacement was attenuated by $\sqrt{a/r}$, where a is the radius of the soil-structure interface and r is the distance from the origin. In addition the true area of the quadrature elements was used. Without the attenuation, a cylindrical plane wave model, the DAA damping results are essentially reproduced.

These results demonstrate that the volume-wave model of Subsection 2.2.2 is highly accurate for elastic medium response. The body-force formulation would therefore be preferred over the DAA formulation, except that it has the following shortcomings. First, the volume integration must enclose all of the medium through which the wave front of the outgoing wave passes. Fortunately, however, large elements can be used; in this problem, for example, 18 radial elements were used to reach 10 cavity radii out into the medium. Second, numerical noise produced by the double-differentiation of displacement was so severe that obtaining a reliable solution was difficult. The only satisfactory results were obtained with quadrature elements of uniform radial dimension and time integration with a small fixed-step. The time increment required to obtain a satisfactory solution was roughly one-fourth that required to obtain a satisfactory solution with the DAA formulation. The explicit central-difference method was much superior to the implicit Park method for solving the body-force equations of motion.

The numerical noise problem discussed above may be circumvented by other strategies; two examples follow. One, the boundary acceleration, obtained from $\ddot{u} = D\dot{q}$, could be propagated into the medium as the boundary displacements are in the VW model. Two, the field acceleration can be computed from a first differentiation of the stress field, i.e., from a force balance. Either of these methods should produce a smoother acceleration field for computational purposes. These methods were not pursued in this study.

3.3 J_2 -THEORY MEDIUM: DAA AND NONSAP RESULTS

This problem involves the elastic-plastic response of an infinite cylindrical cavity surrounded by a J_2 -plasticity theory inelastic medium; see section 3.1 for the elastic response. The cavity has a radius of 25.0 inches. The material properties are $E = 500,000$ psi, $\nu = 0.25$, $C = 200,000$ psi, a von Mises yield stress of 7500 psi, a slope of 50,000 psi after yield (0.1 the elastic slope) and a density of 117 lb/ft³. A J_2 flow rule plasticity model is used for the DAA computations.

This is based on a two element mechanical sublayer model [6]. The excitation is provided by an internal pressure pulse represented by an isosceles triangle with a 17,800 psi peak and a duration of 1.71 msec (2 transit times: 2 diameters). For the cavity, $\underline{M}_s = \underline{K}_s = \underline{Q}$ so the governing equation (11) becomes a first-order equation. Therefore, the implicit integration must be used to solve this problem, as the central-difference explicit integrator is valid only for second-order equations.

The radial displacement response, shown in Figure 7, was computed with both the quasi-static DAA (Subsection 2.2.1) and the quasi-dynamic DAA (Subsection 2.2.2) formulations, for comparison with the NONSAP Finite Element Code [18]. For the quasi-static DAA calculation, the centroids of the volume (area) quadrature elements are located at 28.75, 40.00, 62.50, 107.50, and 197.50 inches. For the first quasi-dynamic DAA calculation, the centroids of the quadrature elements are at 27.50, 32.50, 37.50, 42.50, 47.50, 52.50, 67.50, 82.50, 97.50, 112.50, 127.50, 142.50, 192.50, 242.50, 292.50, 342.50, 392.50 and 442.50 inches. The second quasi-dynamic DAA calculation makes use of only the first 6 quadrature elements characterizing the first quasi-dynamic calculation.

Figure 7 shows that all the DAA formulations produce similar responses. This indicates that the quasi-static and quasi-dynamic models are essentially equivalent for an inelastic J_2 material, and that only a relatively small volume near the soil-structure interface need be considered to obtain a converged solution. Figure 7 also shows that the DAA response peaks are approximately 37% smaller than the NONSAP peak, and that the DAA permanent displacements are approximately 33% smaller than the NONSAP permanent displacement. This compares with the 24.1% underprediction of peak response by the DAA in the elastic case discussed in Subsection 3.1.

This response problem is considered to represent an overly severe test of the DAA for a J_2 material. This is because no embedded structure is included to mitigate inaccuracies introduced by the DAA (cf. Subsection 3.1). In any case, inelastic soil behavior is not described by J_2 plasticity theory, so the more realistic Cap model must be introduced, as described in the following.

3.4 CAP-MODEL MEDIUM: QUASI-STATIC DAA AND TRANAL RESULTS

To provide check cases for the quasi-static DAA formulation of Subsection 2.2.1, the problems shown in Table 1 are considered. These problems were run on the DAA code and the TRANAL code [19]. The material properties used in these calculations are shown in Table 2. The Cap model data [20] was modified slightly to provide an elastic response before yielding by taking $\chi_0 = -R(A-C)$. This modification was nec-

essary to move the J_2 -failure surface up the J_2 -axis; otherwise yielding occurs immediately with the quasi-static DAA formulation.

For these check cases agreement between the DAA and TRANAL responses was nonexistent. For the profile 2 pressure pulse the DAA response predicts $P_e = 4800$ psi, while TRANAL predicts $P_e = 1500$ psi. For the nonlinear calculations at $P_o = 2P_e$ and $5P_e$, the agreement is even poorer. In addition, nonlinear calculations for the same peak pressure are in poor agreement. This poor agreement is characterized by magnitude differences of a factor of 3-10 and the shape of the displacement histories not being similar. The basic reason for the poor comparison is the fact that the quasi-static DAA stress field has no I_1 component for the internal axisymmetric load (see Subsection 2.2.1). For this reason, the quasi-dynamic DAA formulation of Subsection 2.2.2 was developed.

3.5 CAP-MODEL MEDIUM: QUASI-DYNAMIC DAA AND TRANAL RESULTS

These check cases, shown in Table 3, are very similar to the internal-excitation axisymmetric cases considered in Section 3.4. Except a slightly different pressure pulse is used; the reason for this is discussed below. Now the peak pressure is chosen as 7.35 ksi instead of being based on the pressure to cause yielding of the soil. The material properties are also very similar; see Table 4. Now χ_o is -0.0441 ksi as given in [20]. Since the quasi-dynamic DAA is based on reproducing, as best as possible, the actual volume displacement, the modification to χ_o to move the initial yield surface is no longer needed. And with this χ_o there is essentially no elastic response so defining the peak based on P_e is no longer applicable.

Figures 8 and 9 show displacement response histories produced by the quasi-dynamic DAA (Q-D DAA) formulation without "separation", along with corresponding TRANAL response histories [21]. Except at very early times, agreement between the DAA and TRANAL histories is nonexistent. Actually, the histories begin to diverge when tensile cutoff occurs in the TRANAL calculations. This occurs roughly at $t/\tau_{\frac{1}{2}} = 0.5$ for the short pulse and $t/\tau_{\frac{1}{2}} = 2.0$ for the long pulse. The crude DAA separation model of Subsection 2.5 hardly improves the situation, as shown in Figures 10 and 11. Indeed, the DAA results of Figure 11 diverge.

In all of the DAA calculations, the volume (area) integration encompassed a region enclosing the farthest circle reached by the outgoing wave front. For the short pulse, eighteen radial elements were used, with the centroids at 40.57, 42.97, 45.37, 47.77, 50.17, 52.57, 62.17, 71.77, 81.37, 90.97, 100.6, 110.2, 148.6, 187.0,

225.4, 263.8, 302.2, and 340.6 inches. For the long pressure pulse, seventeen radial elements were used, with the centroids at 41.07, 44.47, 47.87, 51.27, 54.67, 58.07, 73.47, 88.87, 104.3, 119.7, 135.1, 150.5, 220.9, 291.3, 361.7, 432.1, and 502.5 inches. The quasi-dynamic Cap-model calculations were quite sensitive to variations in the volume mesh; this is in contrast to the relative insensitivity exhibited in the quasi-dynamic calculations for the J_2 model.

The calculations presented in this subsection were performed with the central-difference explicit time integrator. The explicit integrator was eventually chosen over the implicit one because it was faster and more reliable when confronted with the highly irregular nonlinear soil stiffness forces associated with the tensile cutoff and dilatancy aspects of the Cap model.

3.6 CAP-MODEL MEDIUM: BODY-FORCE RESULTS

The last attempt to obtain reasonable correlation with the TRANAL results involved the body-force formulation discussed in Subsection 2.3.1. The problem solved pertains to the short pressure pulse described in Table 3. Body-force displacement response is compared with TRANAL response in Figures 12 and 13. The correlation between body-force and TRANAL results is seen to be poor. A comparison of Figures 8 and 10 with Figures 12 and 13, respectively, shows that the body-force and quasi-dynamic-DAA formulations produce similar responses, indicating consistency between the two formulations.

To obtain stable body-force solutions, a small fixed time step was used in the explicit integrations and the 18 volume elements were all 20 inches in radial dimension. The "no separation" calculation involved a constant elastic sound speed in the soil, while the "separation" calculation involved a variable sound speed. The variable sound speed option produces the slowly growing instability shown in Figure 13, as discussed in Subsection 2.3.1.

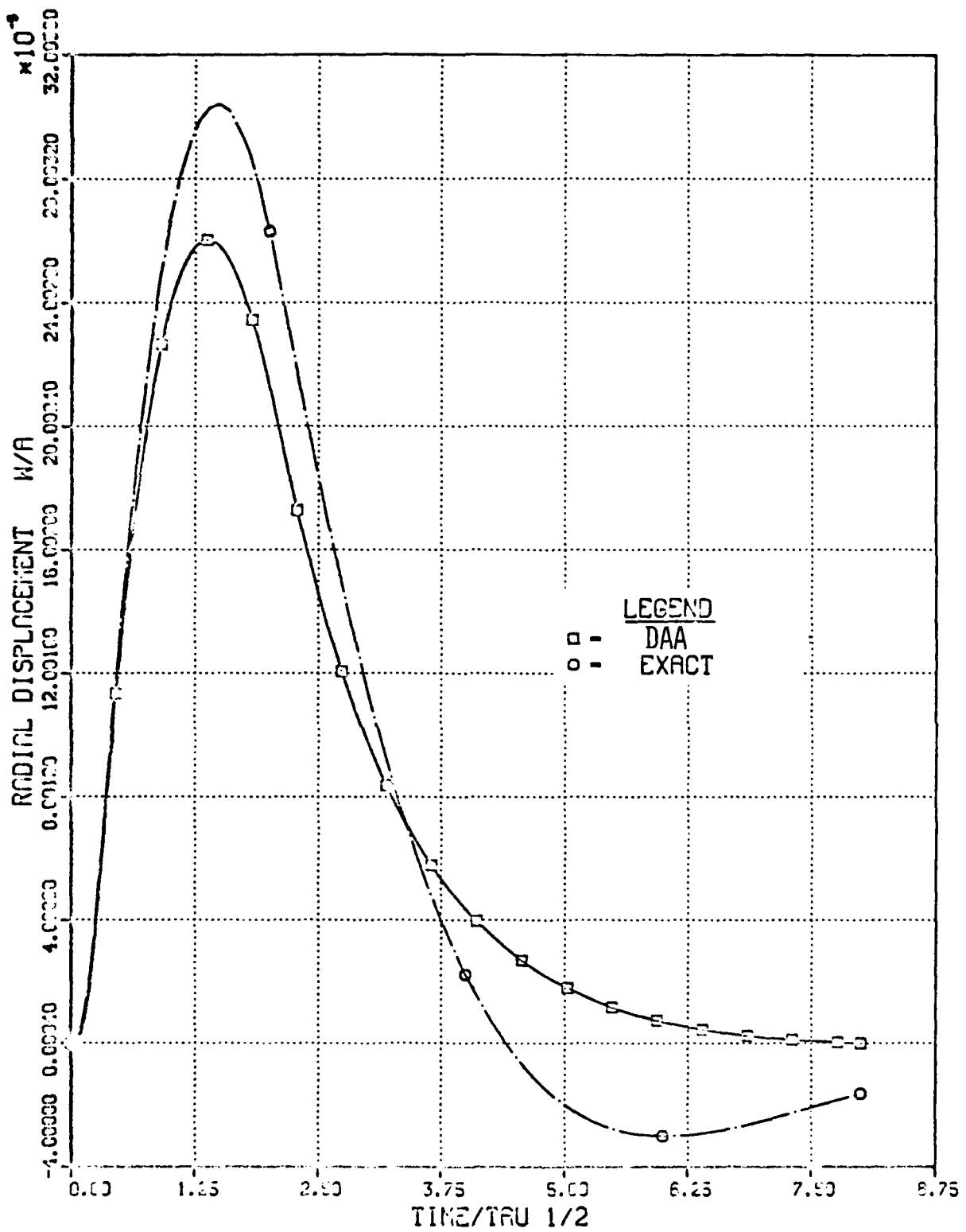


Figure 5. Elastic response: DAA and exact.

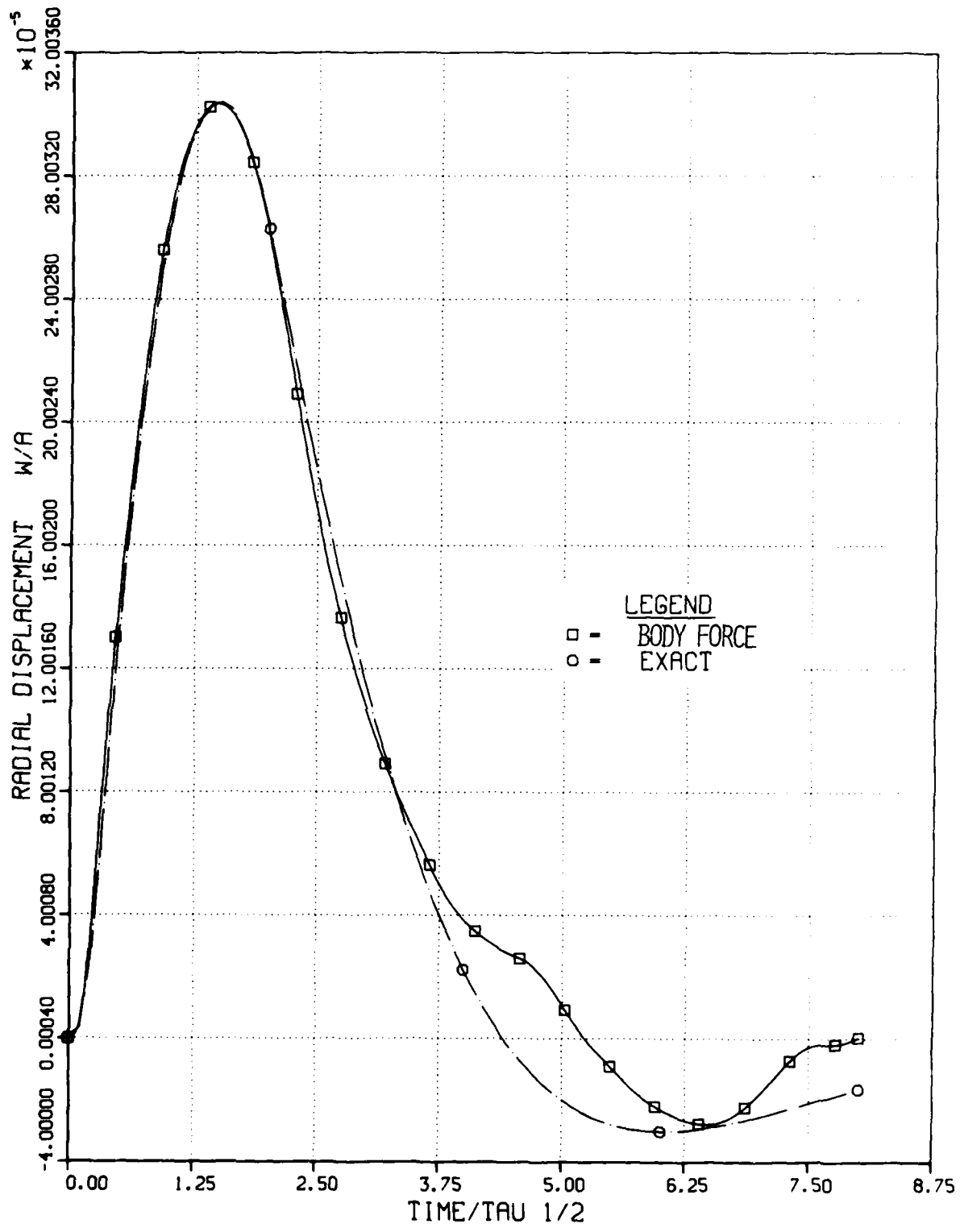


Figure 6. Elastic response: body force damping and exact.

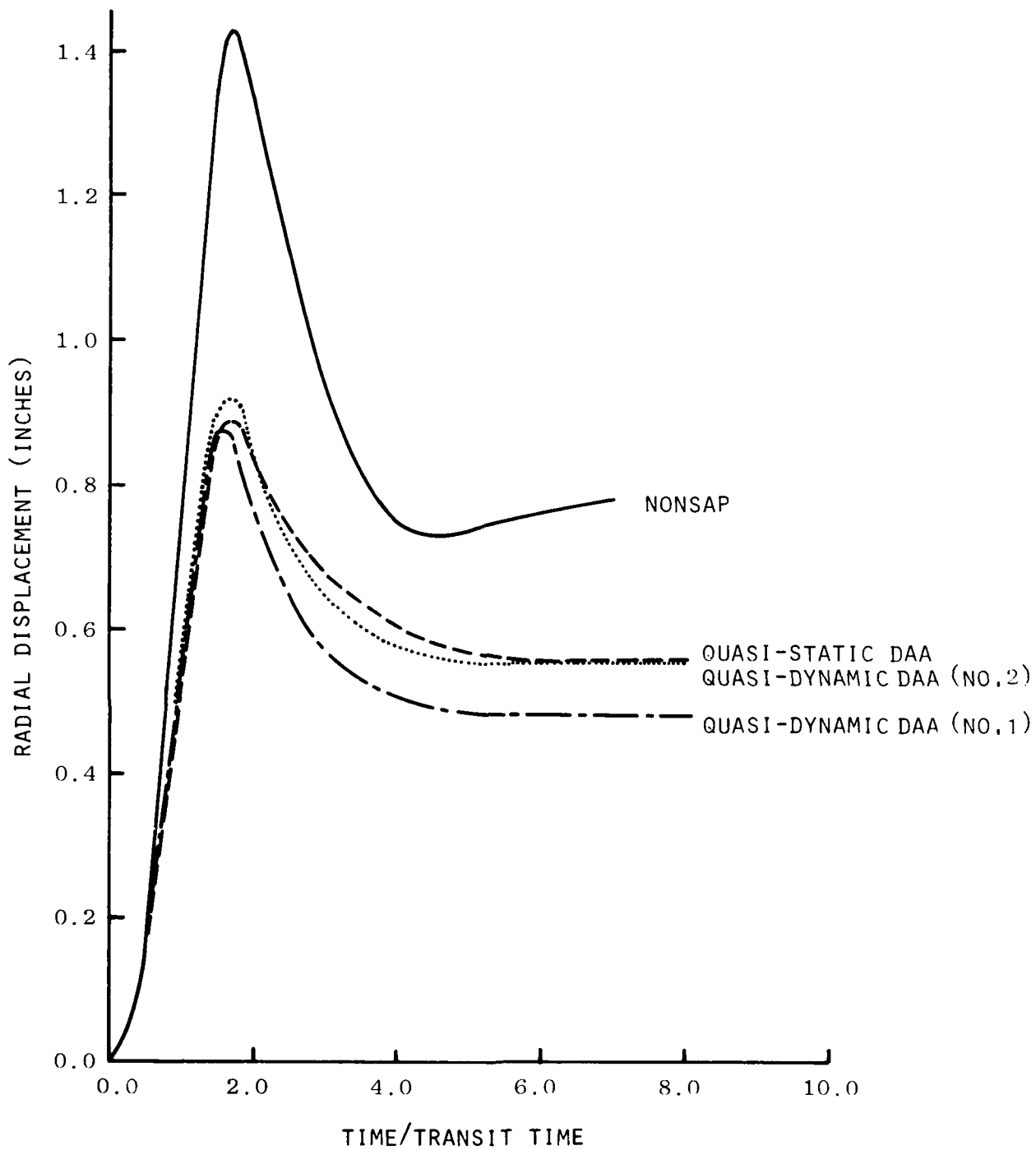


Figure 7. Elastic-plastic J_2 cavity response.

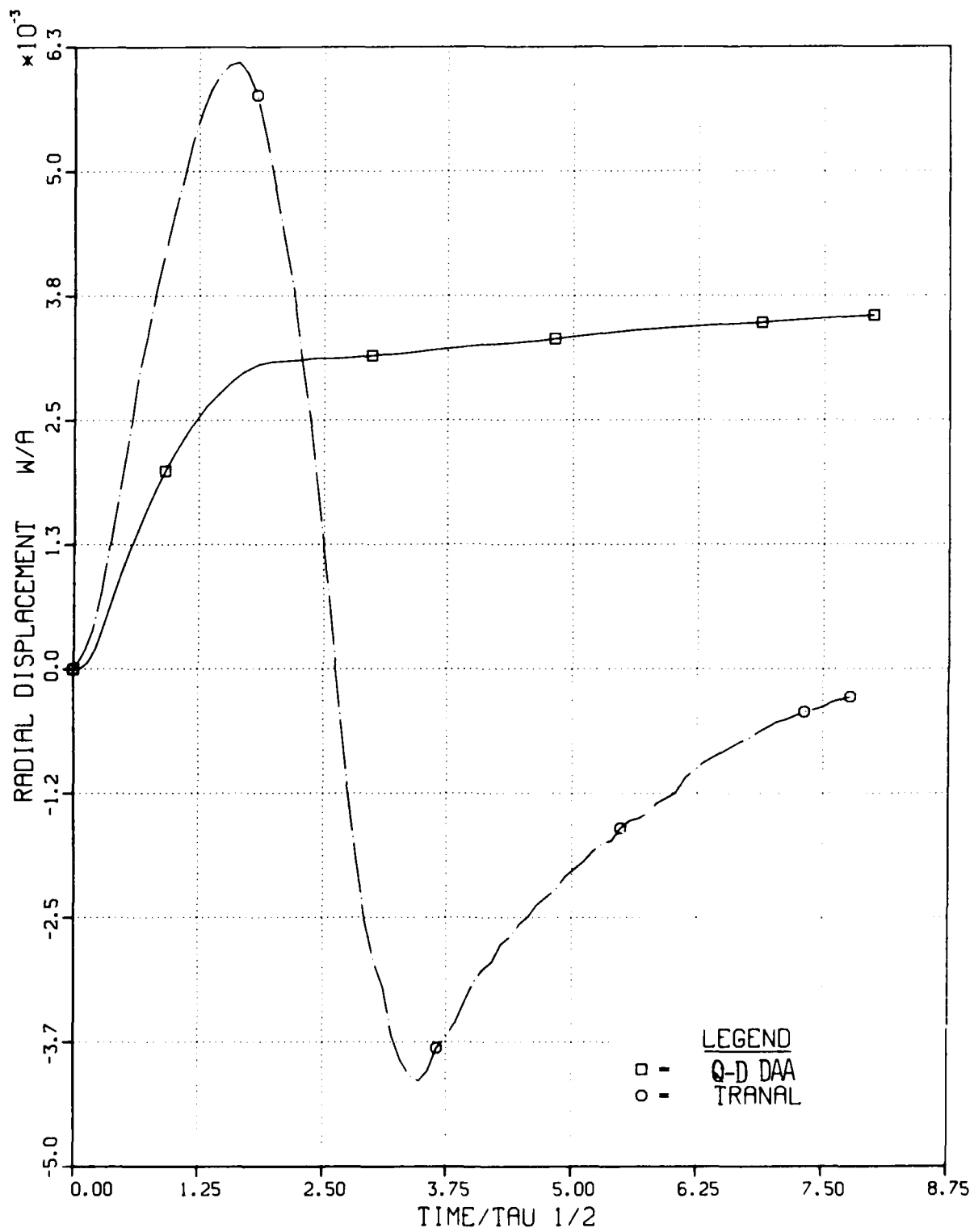


Figure 8. Elastic plastic Cap model response, short pulse.

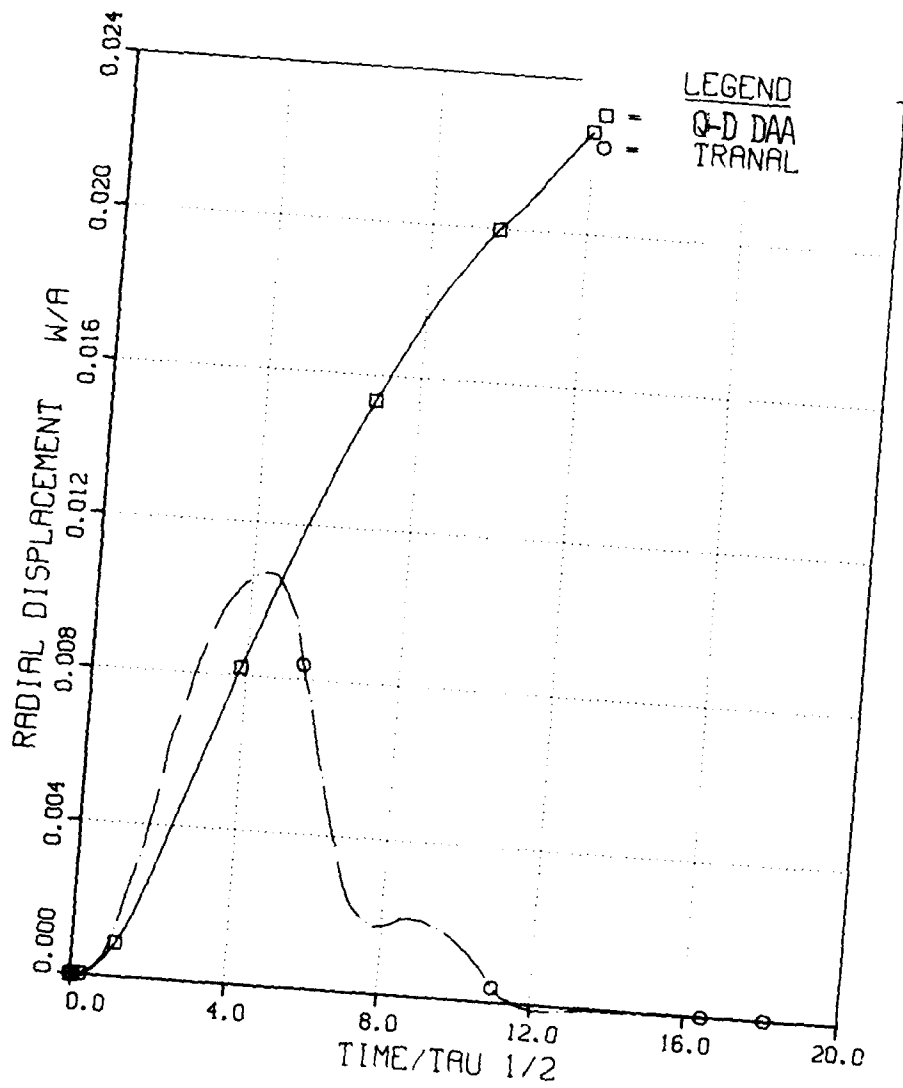


Figure 9. Elastic plastic Cap model response, long pulse.

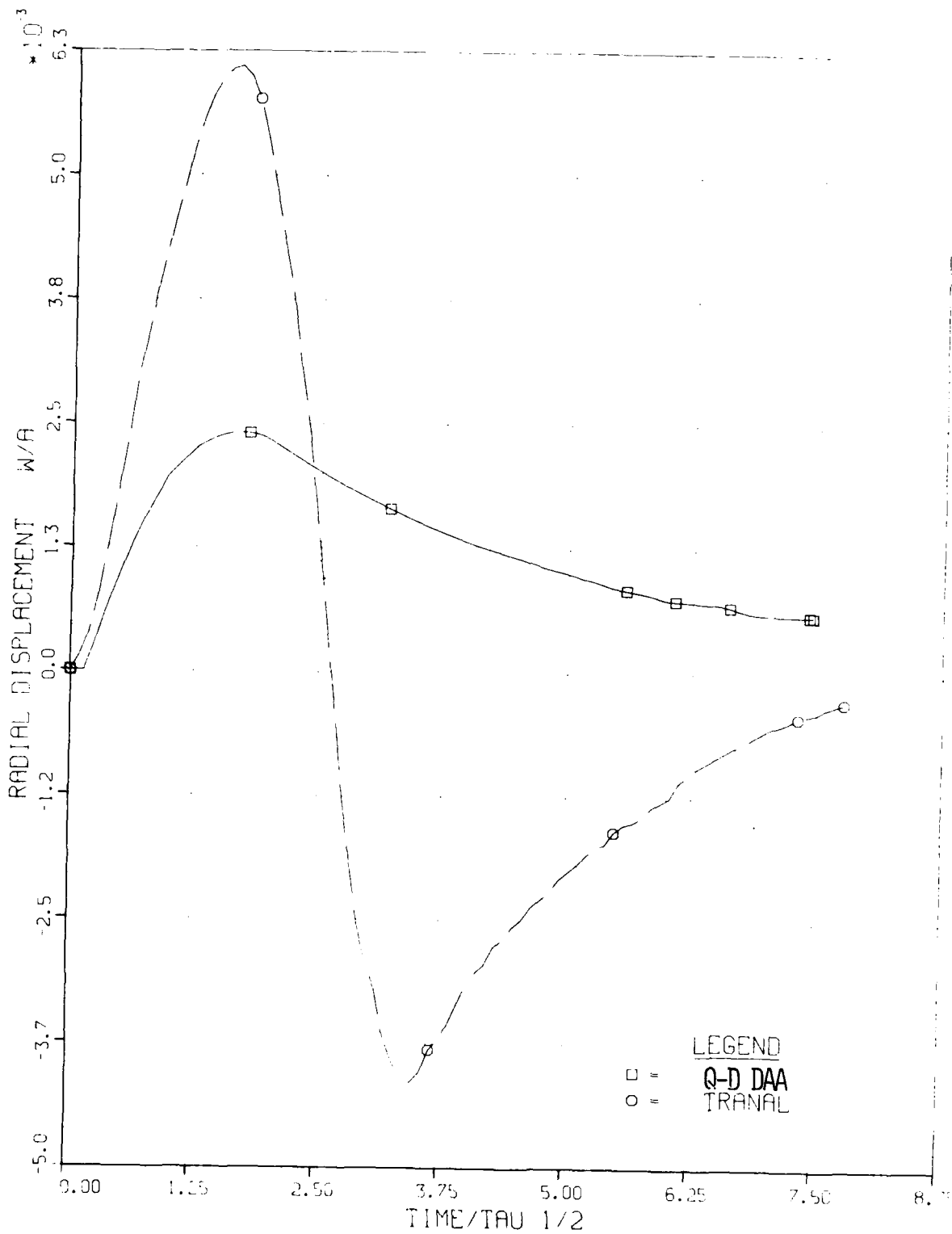


Figure 10. Elastic plastic Cap model response, short pulse, and with "separation".

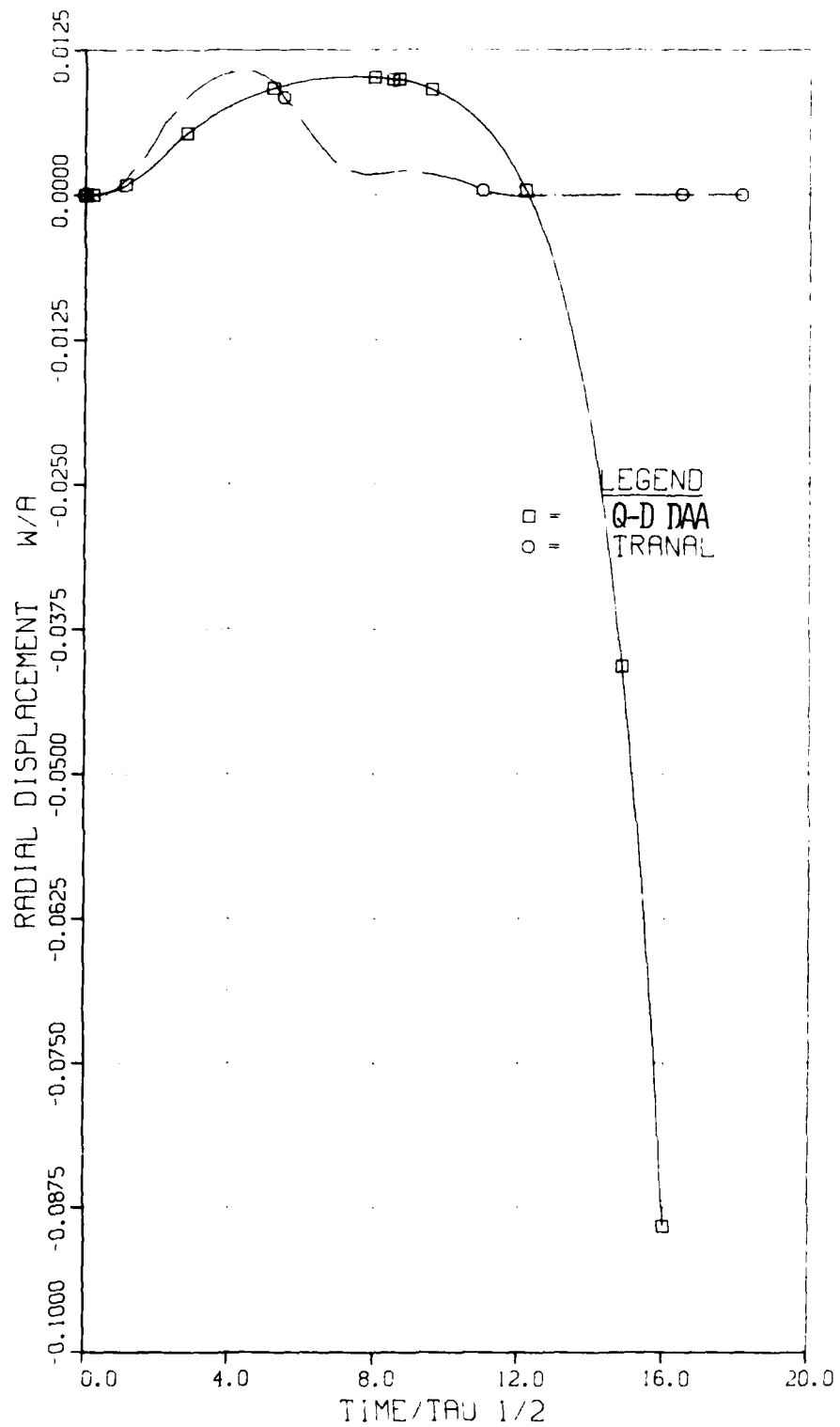


Figure 11. Elastic plastic Cap model response, long pulse, and with "separation".

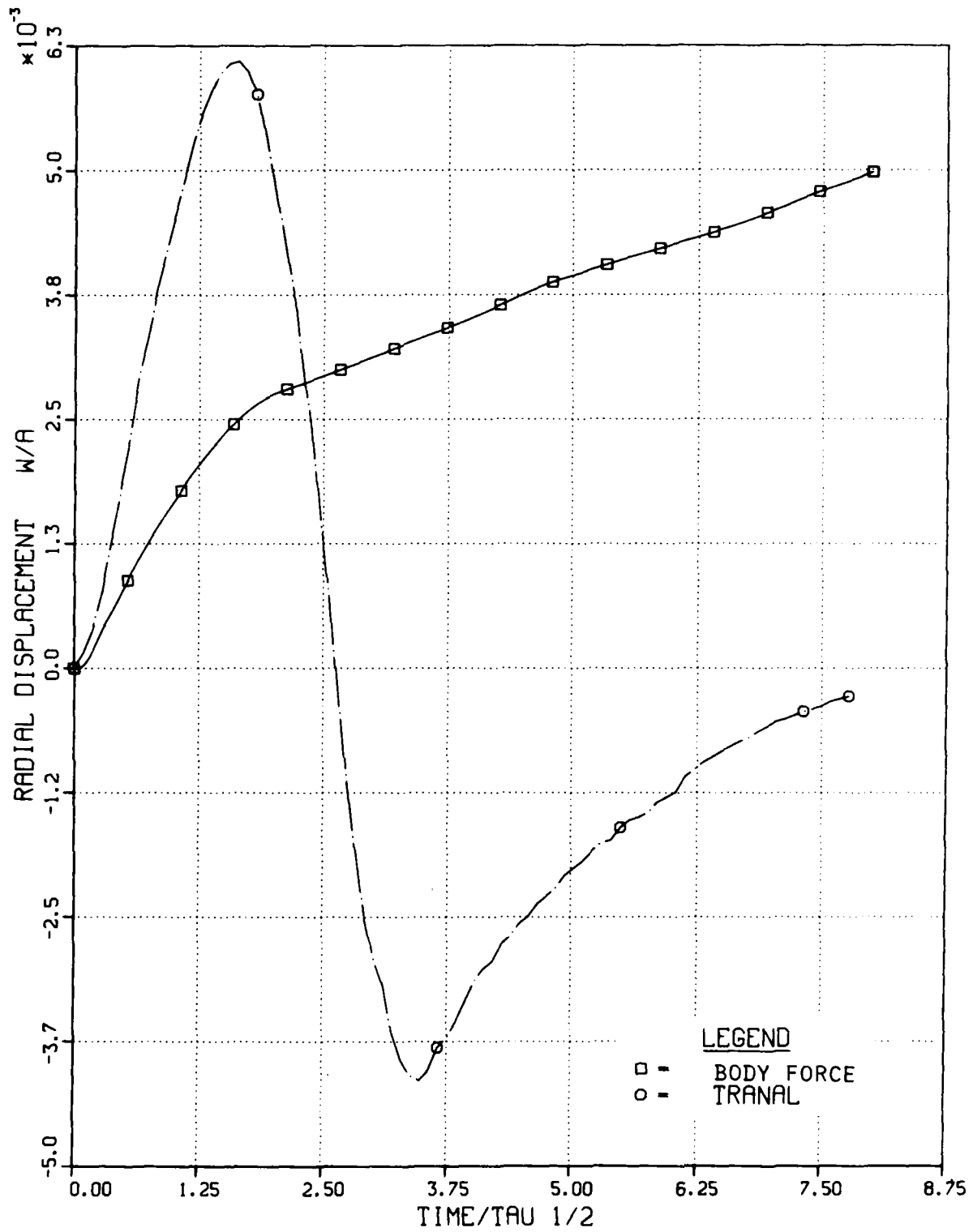


Figure 12. Elastic plastic Cap model response, short pulse, and body force damping.

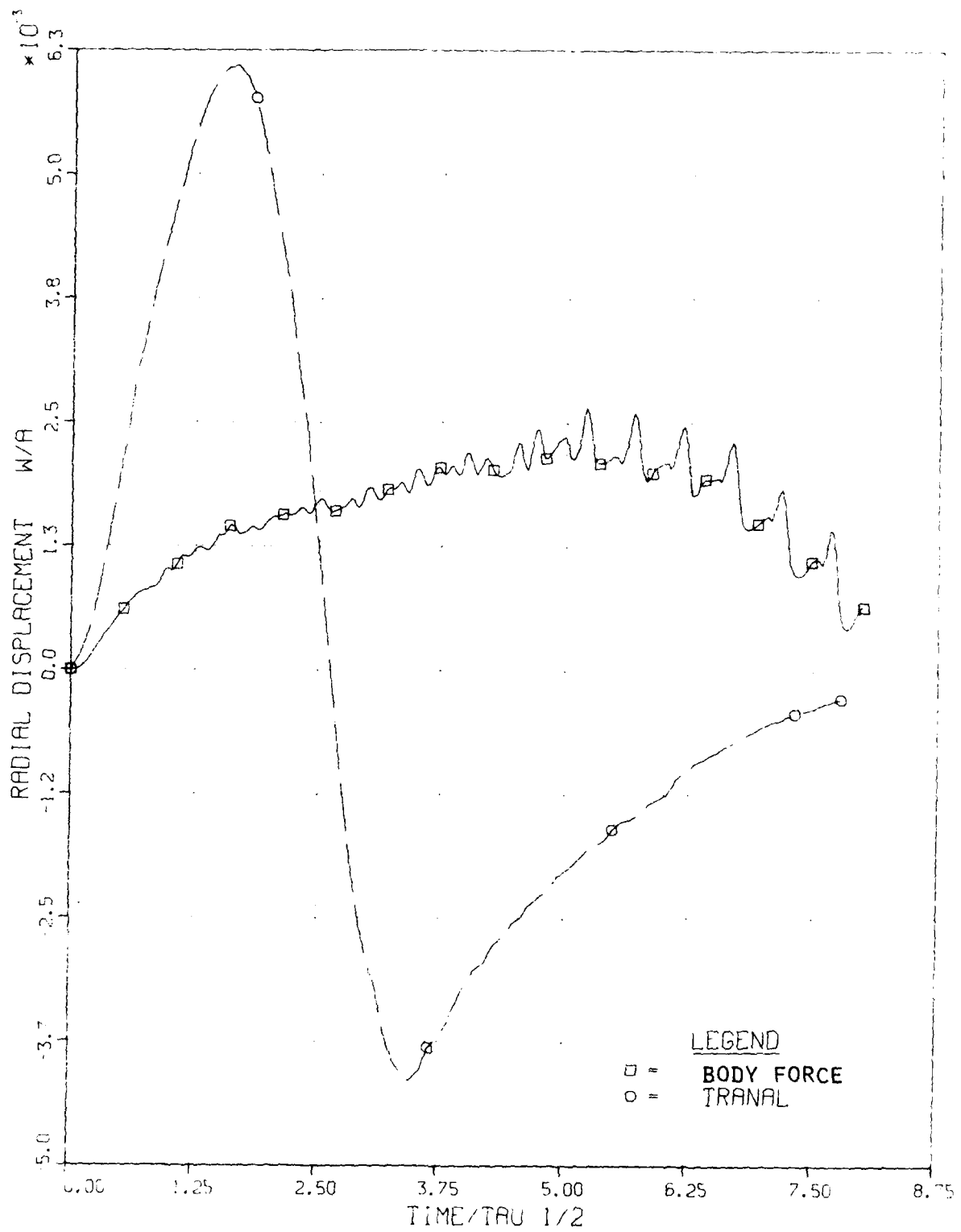
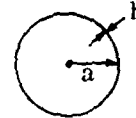


Figure 13. Elastic plastic Cap model response, short pulse, body force damping, and with "separation".

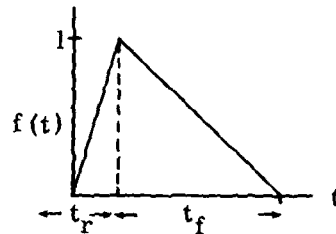
Table 1. DAA-SSI Check Runs: 1

Medium: NTS Tuff (Mighty Epic Model)

Shell: Steel ($\frac{a}{h} = 50$)
 $a = 1\text{m}$ (39.3701 inches)



Excitation: Internal Triangular Pulse
 Internal: $p(\theta, t) = P_o f(t)$



t_d is a convenient delay constant

Large Yield \rightarrow Profile 1: $t_r/t_{\frac{1}{2}} = 2, t_f/t_{\frac{1}{2}} = 8$

Near Surface \rightarrow Profile 2: $t_r/t_{\frac{1}{2}} = 0.2, t_f/t_{\frac{1}{2}} = 1.8$
 Small Yield

$$t_{\frac{1}{2}} = \frac{a}{c_d}$$

Two pressure magnitudes: $P_o/P_e = P_o/P_e = 5$

where P_e is the maximum pressure-loading for which the medium remains elastic.

Thus we have: Four Internal-Excitation Axisymmetric Cases

Table 2. Material Properties

Inelastic Medium NTS Tuff (Mighty Epic Model)

Elastic Portion

$$K = 100 K_b = 1,470 \text{ ksi}$$

$$G = 38 K_b = 559 \text{ ksi}$$

Failure Surface

$$A = 0.5 K_b = 7.36 \text{ ksi}$$

$$B = 0.52 K_b^{-1} = 0.03537 \text{ ksi}^{-1}$$

$$C = 0.44 K_b = 6.486 \text{ ksi}$$

$$TCUT = 0.1 K_b = 1.47 \text{ ksi (tension cutoff)}$$

Cap

$$R = 3$$

$$W = 0.015$$

$$X_o = -2.676 \text{ ksi}$$

Mass Density

$$\rho = 2 \text{ gm/cm}^3 = 3.879 \text{ slug/ft}^3 \text{ (125 \#/ft}^3\text{)}$$

Wave Speeds

$$C_p = 9,100 \text{ fps}$$

$$C_s = 4,560 \text{ fps}$$

Elastic Steel

$$E = 30,000 \text{ ksi}$$

$$G = 11,538 \text{ ksi}$$

$$\nu = 0.3$$

$$\rho = 14.3 \text{ slug/ft}^3 \text{ (460 \#/ft}^3\text{)}$$

$$C_p = 30,166 \text{ fps}$$

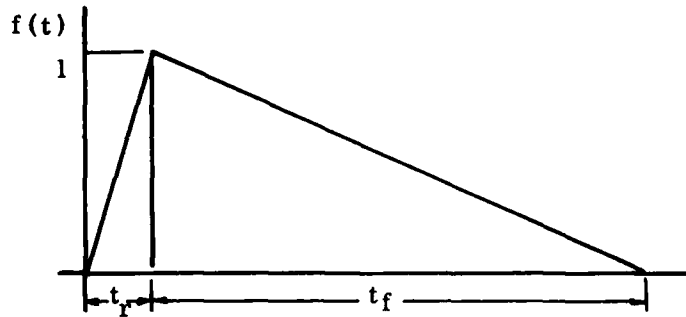
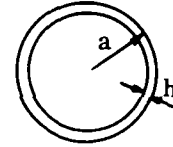
$$C_s = 10,780 \text{ fps}$$

Table 3. DAA-SSI Check Runs: 2

Medium: NTS Tuff (Mighty Epic Model)

Shell: Steel ($a/h = 50$, where $a = 1$ meter = 3.28 feet)

Excitation: Internal Triangular Pulse, Axisymmetric Case
 Internal Pressure $P(t) = P_0 f(t)$
 where $P_0 = \frac{1}{2}Kb = 7.35$ ksi and $f(t)$ is defined as follows:



a. Short Pulse (Small Yield)

$$t_r/t_{\frac{1}{2}} = 0.2, \quad t_f/t_{\frac{1}{2}} = 1.8$$

b. Long Pulse (Large Yield)

$$t_r/t_{\frac{1}{2}} = 2, \quad t_f/t_{\frac{1}{2}} = 8$$

In both cases, $t_{\frac{1}{2}} = a/C_p$, C_p is the wave speed in the medium.

Table 4. Material Properties

Inelastic Medium NTS Tuff (Mighty Epic Model)

Elastic Portion

$$K = 100 \text{ Kb} = 1,470 \text{ ksi}$$

$$G = 38 \text{ Kb} = 559 \text{ ksi}$$

Failure Surface

$$A = 0.5 \text{ Kb} = 7.36 \text{ ksi}$$

$$B = 0.52 \text{ Kb}^{-1} = 0.03537 \text{ ksi}^{-1}$$

$$C = 0.44 \text{ Kb} = 6.468 \text{ ksi}$$

$$D = 1.8 \text{ Kb}^{-1} = 0.12245 \text{ ksi}^{-1}$$

$$\text{TCUT} = 0.1 \text{ Kb} = 1.47 \text{ ksi (tension cutoff)}$$

Cap

$$R = 3$$

$$W = 0.015$$

$$X_o = -0.003 \text{ Kb} = -0.441 \text{ ksi}$$

Mass Density

$$\rho_m = 2 \text{ gm/cm}^3 = 3.879 \text{ slug/ft}^3 \text{ (125 \#/ft}^3\text{)}$$

Wave Speeds

$$C_{pm} = 9,100 \text{ fps}$$

$$C_{sm} = 4,560 \text{ fps}$$

Elastic Steel

$$E = 30,000 \text{ ksi}$$

$$G = 11,538 \text{ ksi}$$

$$\nu = 0.3$$

$$\rho_s = 14.3 \text{ slug/ft}^3 \text{ (460 \#/ft}^3\text{)}$$

$$C_{ps} = 20,166 \text{ fps}$$

$$C_{ss} = 10,780 \text{ fps}$$

SECTION IV

CONCLUSION

The numerical results of the previous section indicate that the doubly asymptotic approximation produces reasonable results for nonlinear medium-structure interaction when the medium obeys a work-hardening J_2 -plasticity theory. For a more realistic soil model (viz., the Cap model), however, reasonable results have not been obtained. In particular, the aspect of the Cap model that creates difficulties for the quasi-static DAA is the hydrostatic-stress invariant I_1 . This impediment led to the introduction of the volume-wave model to create the quasi-dynamic DAA. Unfortunately, the dilatancy and tensile cutoff aspects of the Cap model create difficulties that are not resolved by the quasi-dynamic DAA. An alternative to the DAA, an acceleration body-force approximation based on the volume-wave model, was developed. This approximation, however, possesses marginal numerical stability and yields results that are no better than those produced by the quasi-dynamic DAA.

Perhaps the primary conclusion that may be drawn from this study is that the uniformity assumptions inherent in boundary-element formulations cannot be avoided. Hence, the appearance of dilatancy or tension cutoff, which lead to highly nonuniform material behavior, cannot be tolerated outside the surface to which the DAA is applied. This implies that a DAA may be used outside of a nonuniform region treated with finite-difference or finite-element methods. If hydrostatic-stress effects are negligible outside that region, a quasi-static DAA may suffice. If they are not negligible, a volume-wave model may be required to produce a quasi-dynamic DAA. In the event that internal-forcing problems are satisfactorily treated in this manner, problems involving excitation by incident waves require the use of a wave decoupling approximation such as that discussed in Appendix A.

It is clear from the preceding discussion that boundary-element and infinite-element methods for nonlinear soil-structure interaction analysis are in an embryonic state of development. Furthermore, because of the complexities involved in their formulation and implementation, the prospects for near-term utilization are not very promising. However, the payoff associated with their successful application is sufficiently great that promising ideas for their development should be pursued.

REFERENCES

- [1] P. G. Underwood and T. L. Geers, "Doubly Asymptotic, Boundary-Element Analysis of Dynamic Soil-Structure Interaction", DNA 4512T, Defense Nuclear Agency, Washington, D.C. 20305, 31 March 1978.
- [2] T. L. Geers and C.-L. Yen, "Transient Excitation of an Elastic Cylindrical Shell Embedded in an Elastic Medium: Residual Potential and Doubly Asymptotic Solutions", unpublished.
- [3] J. L. Swedlow and T. A. Cruse, "Formulation of Boundary Integral Equations for Three-Dimensional Elasto-Plastic Flow", Int. J. Solids & Structures, 7, No. 12, 1673-1683, 1971.
- [4] A. Mendelson, "Boundary-Integral Methods in Elasticity and Plasticity", NASA TN D-7418, National Aeronautics and Space Administration, Washington, D.C., November 1973.
- [5] S. Mukherjee, "Corrected Boundary-Integral Equations in Planar Thermoelastoplasticity", Int. J. Solids & Structures, 13, No. 4, 331-335, 1977.
- [6] D. K. Vaughan, "A Comparison of Current Work-Hardening Models used in the Analysis of Plastic Deformations", M.S. Thesis, Texas A & M University, Dec. 1973.
- [7] F. L. Di Maggio and I. S. Sandler, "Material Model for Granular Soils", J. of Engineering Mechanics Div., ASCE, 935-950, June 1971.
- [8] I. Sandler and D. Rubin, "A Modular Subroutine for the Cap Model", DNA 3875F, Defense Nuclear Agency, Washington, D.C. 20305, 2 Jan. 1976.
- [9] J. D. Achenback, Wave Propagation in Elastic Solids, North-Holland Publ. Co., Amsterdam, 1973.
- [10] P. Bettess, "Infinite Elements", Int. J. Num. Meth. Engng., 11, 53-64, 1977.
- [11] O. C. Zienkiewicz, D. W. Kelly, and P. Bettess, "The Coupling of the Finite Element Method and Boundary Solution Procedures", Int. J. Num. Meth. Engng., 11, 355-375, 1977.
- [12] P. G. Underwood and K. C. Park, "Implementation of a Variable-Step Integration Technique for Nonlinear Structural Dynamic Analysis", Proceedings of the 4th International Conference on Structural Mechanics in Reactor Technology, San Francisco, CA, 15-19 August 1977.
- [13] K. C. Park and P. G. Underwood, "A Variable-Step Central Difference Method for Structural Dynamic Analysis, Part I - Theoretical Aspects", LMSC-D626686, Lockheed Palo Alto Research Laboratory, Palo Alto, CA, July 1978.
- [14] P. G. Underwood and K. C. Park, "A Variable-Step Central Difference Method for Structural Dynamic Analysis, Part II - Implementation and Performance Evaluation", LMSC-D633782, Lockheed Palo Alto Research Laboratory, Palo Alto, CA, December 1978.

- [15] O. C. Zienkiewicz, The Finite Element Method in Engineering Science, McGraw-Hill, London, 1971.
- [16] S. P. Timoshenko and J. N. Goodier, Theory of Elasticity, 3rd Ed., Mc-Graw-Hill, New York, 1970.
- [17] W. A. Loden and L. E. Stearns, "User's Manual for the REXBAT Program", LMSC-D460265, Lockheed Missiles and Space Co., Sunnyvale, CA, January 1976.
- [18] J. Crawford and R. N. Murtha, Private Communication, NCL, February 1977.
- [19] S. Pang, Private Communication, Weidlinger Associates, Menlo Park, CA, Dec. 1977.
- [20] J. Sweet, "Dynamic Response of Underground Structures", Systems, Science and Software, La Jolla, CA, SSS-R-76-2829, January 1976.
- [21] S. Pang, Private Communication, Weidlinger Associates, Menlo Park, CA, June 1978.
- [22] T. A. Cruse and F. J. Rizzo, eds., Boundary Integral Equation Method: Computational Applications in Applied Mechanics, AMD-Vol. 11, ASME, New York, 1975.
- [23] F. J. Rizzo, "An Integral Equation Approach to Boundary Value Problems of Classical Elastostatics", Quart. Appl. Math., 25, 83-95, 1967.
- [24] C. S. Desai and J. F. Abel, Introduction to the Finite Element Method, Van Nostrand Reinhold Company, New York, 1972.
- [25] P. C. Riccardella, "An Implementation of the Boundary-Integral Technique for Planar Problems in Elasticity and Elasto-Plasticity", Ph.D. Thesis, Carnegie-Mellon University, 1973.
- [26] M. Abramowitz and I. A. Stegun, eds., Handbook of Mathematical Functions, Dover Publications, Inc., New York, 1965.

APPENDIX A

WAVE DECOUPLING APPROXIMATION

This appendix presents a brief discussion of the approximation introduced into the DAA from the decomposition of surface forces and displacements into incident and scattered wave components. A simple bar model, which illustrates the physics, is considered.

The basic concept underlying the soil-structure interaction model presented here is the replacement of the effectively infinite volume of medium surrounding the structure by an interface surface that provides to the structure an approximate representation of the dynamic behavior of the medium. This representation is one that approaches exactness in both the low-frequency and high-frequency limits; hence the name "doubly asymptotic approximation". An associated concept is the decomposition of surface forces and displacements into two sets, one pertaining to the incident wave (f_I, u_I) and the other pertaining to the scattered wave (f_S, u_S). In this connection, a second approximation is introduced, viz., a "wave decoupling approximation" (WDA), which will now be described.

Figure A-1 shows a rigid mass embedded in a grounded vertical bar that is loaded at the top by a slowly varying "incident" force f_I . The bar material has zero mass density and exhibits bilinear-hysteretic constitutive behavior. The graph labeled "exact" shows the stress-strain trajectory for a point just below the mass at eight incremental stages of the loading process. The graph labeled "approximate" shows the corresponding trajectory produced by the WDA, as follows. A load increment Δf_I is applied to the bar with the "scattered" force $f_S = Mg$ neglected; this leads to Point 1' on the trajectory. The force f_S is then considered, which leads to Point 1 on the trajectory. An additional load increment is applied to the bar with f_S neglected; this leads to Point 2'. Then the force f_S is again considered, which leads to Point 2. This process continues until Points 6' and 6 are reached; a load increment Δf_I is then subtracted from $f_I = 6\Delta f_I$, which leads to Points 7' and 7. Finally, another load increment Δf_I is subtracted from $f_I = 5\Delta f_I$, which leads to Points 8' and 8.

The trajectories of Figure A.1 indicate that the WDA is in error only during unloading, where path-dependent constitutive behavior becomes manifest. This implies that the WDA should be accurate during the loading phase of a multi-dimensional dynamic interaction analysis for a structure whose bulk stiffness and mass properties are comparable to or greater than those of the surrounding medium. In any case, the WDA

should be accurate when f_S is much smaller than f_I . Because f_S decreases with increasing distance from the surface of a 2-D or 3-D structure, improved accuracy may therefore be obtained by moving the interface surface out from the structure's surface, treating the medium thus enclosed as part of the structure.

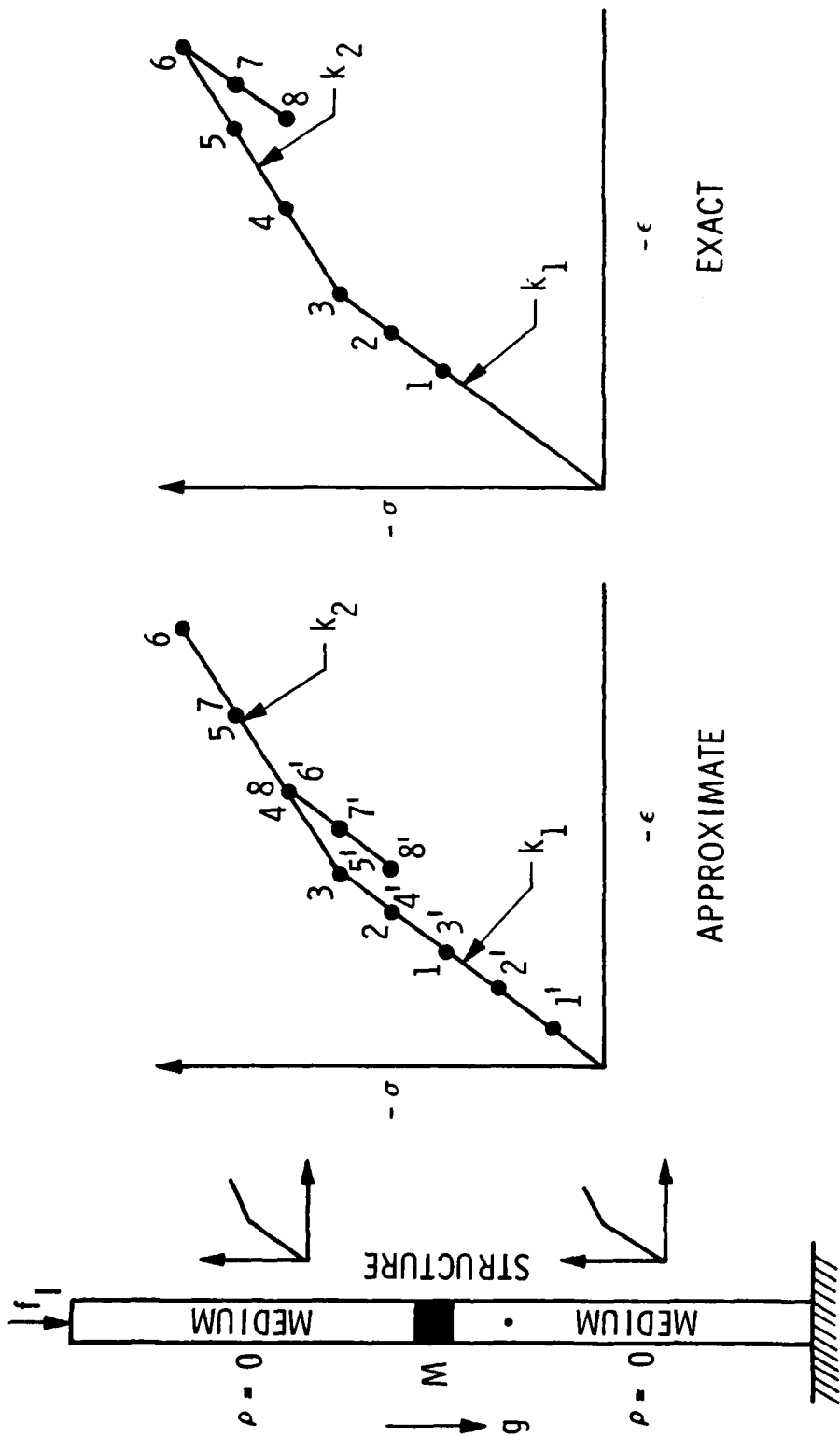


Figure A-1. 1-D quasi-static problem.

APPENDIX B

OUTLINE OF THE DERIVATION OF THE
BOUNDARY INTEGRAL EQUATION FOR INELASTIC MEDIUM

This appendix outlines the initial steps in the derivation of the boundary integral equation for an inelastic medium (5). The derivation is carried out to the point at which other investigators [3,4] have incorrectly neglected a term, as pointed out by Mukerjee [5]. The steps that involve the boundary integral equation itself are not presented as the use of Kelvin's solution, Betti's reciprocal theorem and the divergence theorem to obtain this equation has been thoroughly studied [3,4,5,22,23].

The total strain ϵ_{ij} is written as the sum of the elastic and plastic strain to give

$$\epsilon_{ij} = \epsilon_{ij}^e + \epsilon_{ij}^p \quad (B-1)$$

The total strain is related to the displacement by the linear kinematic relation

$$\epsilon_{ij} = (u_{i,j} + u_{j,i})/2 \quad (B-2)$$

In [3,4] the volumetric plastic strain ϵ_{kk}^p is assumed to be zero; an incorrect assumption for two-dimensional plane strain [5] and for three-dimensional plasticity theory involving volumetric changes, such as the Cap model [7]. Here the assumption

$$\epsilon_{kk}^p \neq 0 \quad (B-3)$$

is made. Hence, from Hooke's law, (B-1), (B-2) and (B-3) the stress σ_{ij} becomes

$$\sigma_{ij} = \lambda u_{k,k} \delta_{ij} + \mu (u_{i,j} + u_{j,i}) - \lambda \epsilon_{kk}^p \delta_{ij} - 2\mu \epsilon_{ij}^p \quad (B-4)$$

where λ and μ are the Lamé coefficients. Finally, from the equilibrium equation

$$\sigma_{ij,j} = -b_i \quad (B-5)$$

and (B-4) the Navier equation for inelastic medium becomes

$$u_{i,jj} + \frac{1}{(1-2\nu)} u_{k,ki} = 2\epsilon_{ij,j}^p + \frac{2\nu}{1-2\nu} \epsilon_{kk,i}^p - \frac{b_i}{G} \quad (B-6)$$

where $G = \mu$ and Poisson's ratio, $\nu = \lambda/2(\lambda+\mu)$.

The two basic paths to follow in the boundary integral equation derivation start with Betti's reciprocal theorem and use (B-4) [3] or start with B-6 [4]. In both

cases the underlined term is not included in [3,4], but Mukherjee [5] presents a correct derivation of the kernels.

As the only difference occurs in the plastic strain term the kernels for the tractions, displacements and body force in (7) remain unchanged from the linear theory. For two-dimensional plane strain they are [1,22,23]

$$T_{ij}^{k\ell} = \frac{C_3}{r_{ij}} \left[\frac{\partial r_{ij}}{\partial n_j} \left(\delta_{k\ell} C_4 + 2r_{ij,k} r_{ij,i} \right) + C_4 \left(n_j^k r_{ij,\ell} - n_j^\ell r_{ij,k} \right) \right], \quad (B-7)$$

$$U_{ij}^{k\ell} = C_1 \left(\delta_{k\ell} C_2 \ell n r_{ij} - r_{ij,k} r_{ij,\ell} \right), \quad (B-8)$$

and the correct Σ kernel (8) is given by Mukerjee [5] as

$$\Sigma_{ij}^{\ell mk} = -C_3 \left[C_4 \left(\delta_{k\ell} r_{ij,m} + \delta_{mk} r_{ij,\ell} \right) - \delta_{\ell m} r_{ij,k} + 2r_{ij,k} r_{ij,\ell} r_{ij,m} \right] \quad (B-9)$$

where C_1, C_2, C_3 and C_4 are material constants, r_{ij} is the distance from a node point on the i -th element to the variable (field) point of integration on the j -th element, n_j is the unit normal to the surface of the j -th element, n_j^k is the cosine of the angle between n_j and the k -th Cartesian direction, $\delta_{k\ell}$ is a Kronecker delta, and a subscript following a comma represents spatial differentiation with respect to the indicated cartesian coordinate at point j .

Equation (B-9) is valid for two-dimensional plane strain. Also, the Σ kernel given in [3] for the three-dimensional case is incorrect for plasticity which includes volumetric strain.

APPENDIX C

NUMERICAL EVALUATION OF NONLINEAR COEFFICIENT MATRICES

This appendix discusses the numerical approach used to evaluate the integral in (8) to determine the matrix elements $B_{ij}^{\ell mk}$. The evaluation of the first two integrals in (7) was presented in [1] and the integrals in the third of (7) and (13) and (14) follow the approach presented here, so they are not explicitly considered.

As the shape function $\eta_j^{\ell m}$ in (8) is chosen to be 1 the integral (8) reduces to

$$B_{ij}^{\ell mk} = \int_{A_j} \Sigma_{ij}^{\ell mk} dA_j \quad (C-1)$$

and from Appendix B

$$\begin{aligned} \Sigma_{ij}^{\ell mk} = & - \frac{1}{4\pi(1-\nu)r_{ij}} \{ (1-2\nu)(\delta_{k\ell} r_{ij,m} + \delta_{mk} r_{ij,\ell}) \\ & - \delta_{\ell m} r_{ij,k} + 2r_{ij,k} r_{ij,\ell} r_{ij,m} \} \end{aligned} \quad (C-2)$$

where

$$\begin{aligned} r_{ij} &= [(x_{1j} - x_{1i})^2 + (x_{2j} - x_{2i})^2]^{\frac{1}{2}}, \\ r_{ij,k} &= (x_{kj} - x_{ki})/r_{ij}, \end{aligned}$$

$\delta_{k\ell}$, etc., are Kronecker deltas and $i, j, k, \ell, m = 1, 2$. The geometry associated with the integration is shown in Figure C-1. This illustrates that the index i pertains to a fixed node point and the index j pertains to a point within the quadrature element A_j . Note, r_{ij} is the distance between the points i and j and for a specific r_{ij} , $r_{ij,k}$ is the cosine ($k=1$) and sine ($k=2$) of the angle between the x_1 -global axis and the line r_{ij} . The quadrature element is defined as an eight node (parabolic interpolation) curvilinear quadrilateral. This representation allows, where applicable, direct usage of finite element numerical integration methods and in other situations a convenient method for describing the geometry through the shape functions. In this example the plastic strains are evaluated at the center of element (the point 0 in Figure C-1) and assumed to be uniform over A_j , as discussed in Section 2.2.

Three distinct cases arise in the integration of (C-1): 1) i is not in A_j (including the boundary) and $\alpha \neq \beta$ (see Figure C-1); 2) i is not in A_j and $\alpha = \beta$ and

3) i is in A_j . Case 1 is easily integrated by standard numerical integration formulas over the square shown in the upper-righthand corner of Figure C-1. That is, for integration purposes, the curvilinear quadrilateral is mapped onto the square, a standard method in finite element analysis; see [24] for example. Here both one-point ($\xi = \eta = 0$) and four-point ($\xi = \eta \pm \sqrt{\frac{1}{3}}, \pm \sqrt{\frac{1}{3}}$) discrete integrations were found to produce 3 to 4 figure accuracy. The four-point integration rule was used during the latter stages of the study, but generally the one-point integration rule is sufficient. For r_{ij} (j at the centroid 0) greater than the minimum arc length from $i+1$ to i or i to $i-1$, the general rule would be to use one-point integration, otherwise use four-point integration.

Cases 2 and 3 are covered by the same method. Here the basic problem is the singularity in the integrand (C-2) for case 3. The problem for case 2 appears to come from the even-odd behavior of the integrand when $\alpha = \beta$. The method that resolves the case 3 singularity problem also resolves the case 2 difficulty, so they are treated together. To eliminate the singularity, $1/r_{ij}$, the integration over A_j is changed to polar coordinates ρ, θ with the origin at i [25] (see Figure C-2). The $r_{ij,k}$ terms are functions of θ ; see discussion below (C-2), so (C-1) now has the form

$$B = \int_{\theta} \int_{\rho} \frac{1}{r} f(\theta) \rho d\rho d\theta \quad (C-3)$$

Note that, with this polar coordinate system $\rho = r$, hence (C-3) becomes

$$B = \int_{\theta} \int_{\rho} f(\theta) d\rho d\theta, \quad (C-4)$$

so the singularity is removed. The integration (C-4) is carried out over the four triangles shown in Figure C-2. For i on the boundary of A_j only 3 or 2 triangles are needed to cover A_j . Also, note that, $f(\theta) = r_{ij} \Sigma_{ij}^{lmk}$ [see equation (C-2)]. The integral (C-4) is evaluated by applying the three-point one-dimensional Gaussian quadrature rule [26] first to $d\rho$ and then $d\theta$. The three-point rule is used as it produces accuracy comparable to case 1.

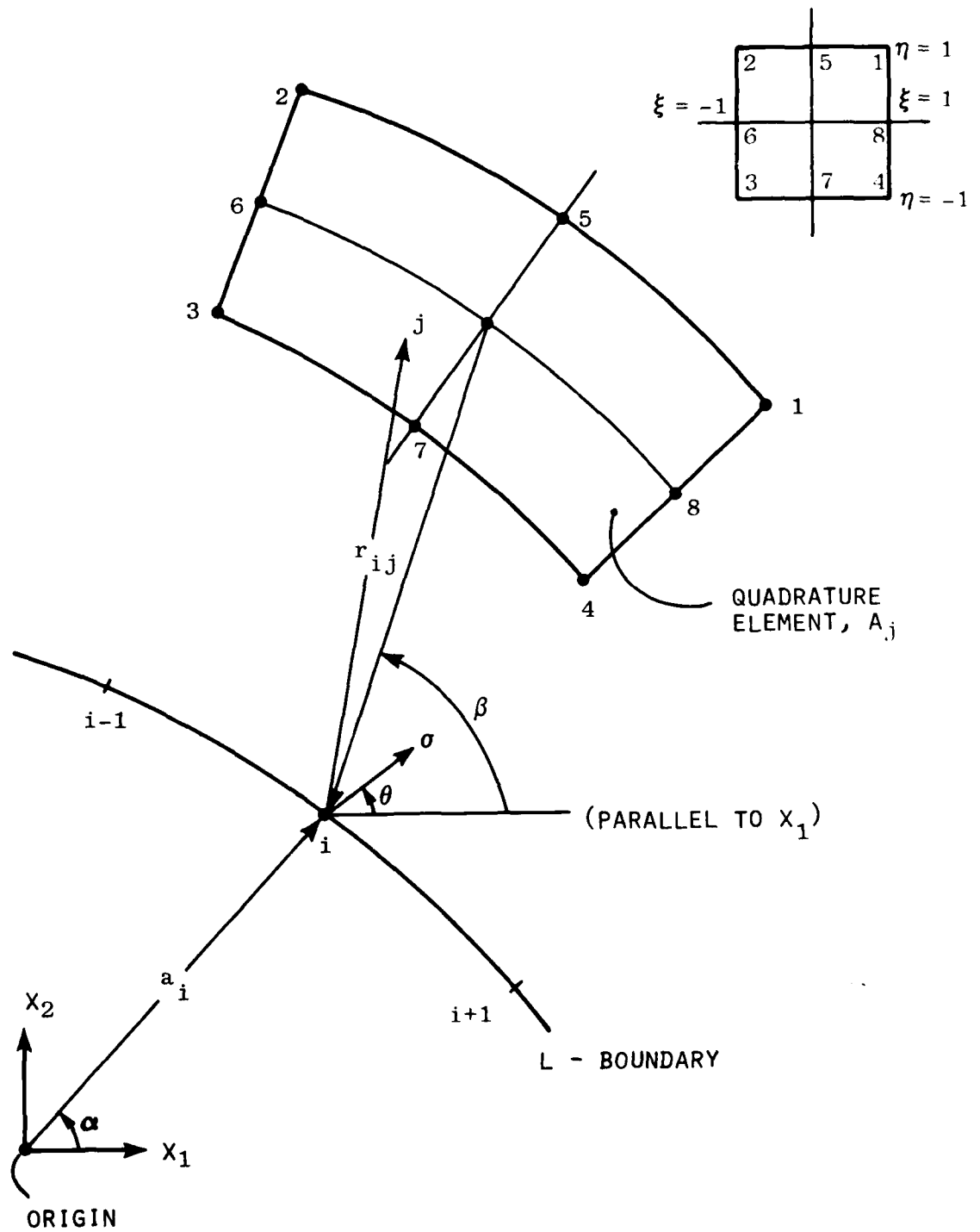


Figure C-1. Area integration element definition.

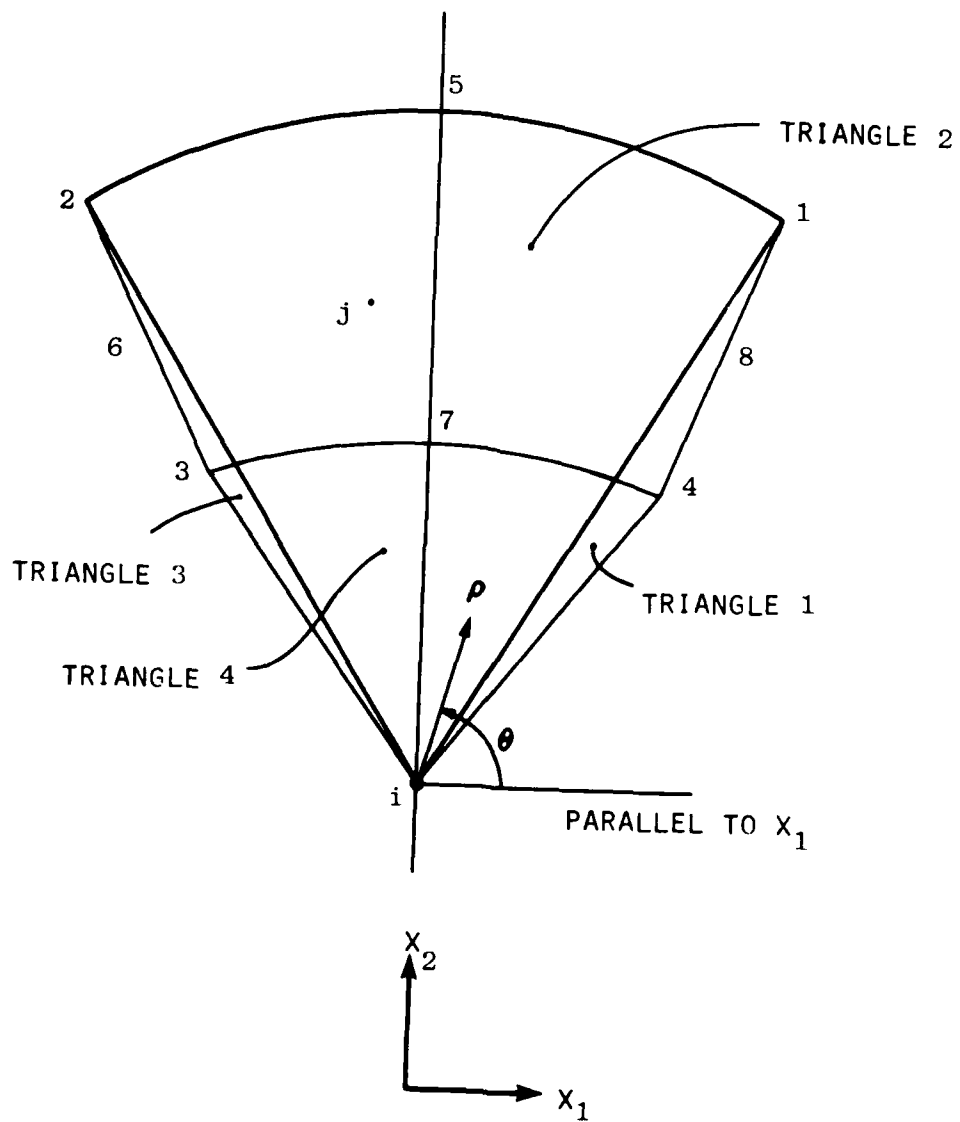


Figure C-2. Geometry for cases 2 and 3.

APPENDIX D

BOUNDARY INTEGRAL EQUATION MATRICES
WITH SYMMETRY CONDITIONS

In this appendix the formulation of boundary integral equation matrices for a symmetry condition is presented. To illustrate the formulation the derivation of the linear stiffness matrix for a symmetry condition is considered. The other matrices, $\underline{\mathcal{S}}$ and $\underline{\mathcal{E}}$, are treated similarly, so they are not considered here.

The formulation is best illustrated by considering the simple example shown in Figure D-1, the x_2 -axis being an axis of symmetry. Matrices are to be formulated for only one-half the problem such that the symmetry condition is properly represented. The node points are selected as shown, such that two nodes are on the symmetry axis, e.g., nodes 1 and 11 in this example. Note, that to obtain the same response from the half (symmetry) model as from the full model, the half model tractions must be one-half the full model tractions but the displacements are equal at nodes 1 and 11. Thus, the sum of the two half models produces the full model. For the two half models the matrix equation for displacements and tractions may be written as

$$\begin{bmatrix} \underline{\mathcal{S}}_{11} & \underline{\mathcal{S}}_{12} \\ \underline{\mathcal{S}}_{21} & \underline{\mathcal{S}}_{22} \end{bmatrix} \begin{Bmatrix} \underline{u}_r \\ \underline{u}_e \end{Bmatrix} = \begin{bmatrix} \underline{\mathcal{E}}_{11} & \underline{\mathcal{E}}_{12} \\ \underline{\mathcal{E}}_{21} & \underline{\mathcal{E}}_{22} \end{bmatrix} \begin{Bmatrix} \underline{t}_r \\ \underline{t}_e \end{Bmatrix} \quad (D-1)$$

where the subscript r indicates the retained degrees of freedom and the subscript e indicates the degrees of freedom eliminated by applying the symmetry condition. The submatrices in (D-1) are composed of the following elements:

- $\underline{\mathcal{S}}_{11}$: The first 22 rows and columns of $\underline{\mathcal{S}}$ (Note, there are 22 rows because there are 11 nodes and 2 DOF/node)
- $\underline{\mathcal{S}}_{12}$: The first 22 rows and the last 20 columns of $\underline{\mathcal{S}}$ and the last 2 columns of $\underline{\mathcal{S}}_{12}$ are the first 2 columns and 22 rows of $\underline{\mathcal{S}}$.
- $\underline{\mathcal{S}}_{21}$: The first 20 rows and 22 columns are the last 20 rows and first 22 columns of $\underline{\mathcal{S}}$ and the last 2 rows and 22 columns are the first 2 rows and 22 columns of $\underline{\mathcal{S}}$.
- $\underline{\mathcal{S}}_{22}$: The first 20 rows and columns are the last 20 rows and columns of $\underline{\mathcal{S}}$, the last 2 rows and 20 columns are the first 2 rows and last 20 columns of $\underline{\mathcal{S}}$, the last 2 columns and 20 rows are the first 2 columns and

the last 20 rows of \underline{S} , and the last 2 rows and 2 columns are the first 2 rows and columns of \underline{S} .

For \underline{E}_{11} , \underline{E}_{12} , \underline{E}_{21} and \underline{E}_{22} the arrangement of elements based on \underline{F} are identical to \underline{S}_{11} , \underline{S}_{12} , \underline{S}_{21} and \underline{S}_{22} with an exception. The exception is that the elements of the first and last two columns of each of the four submatrices are divided by two; this accounts for the one-half value of the traction. In the above \underline{S} and \underline{F} refer to the full problem matrices; see equation (6).

The e-degrees of freedom are related to the r-degrees of freedom by

$$\underline{u}_e = \underline{T} \underline{u}_r \quad \text{and} \quad \underline{t}_e = \underline{T} \underline{t}_r \quad (\text{D-2})$$

where the transformation matrix \underline{T} imposes the symmetry condition. For this problem the components in the x_1 -direction are equal in magnitude and opposite in sign and the components in the x_2 -direction are equal in magnitude and sign. Thus, \underline{T} is a very sparse matrix composed of + and - 1's.

Enforcing the equivalence of virtual work for the full model and the symmetry model gives

$$\underline{S}_r = \underline{S}_{11} + \underline{S}_{12} \underline{T} + \underline{T}^T \underline{S}_{21} + \underline{T}^T \underline{S}_{22} \underline{T} \quad (\text{D-3})$$

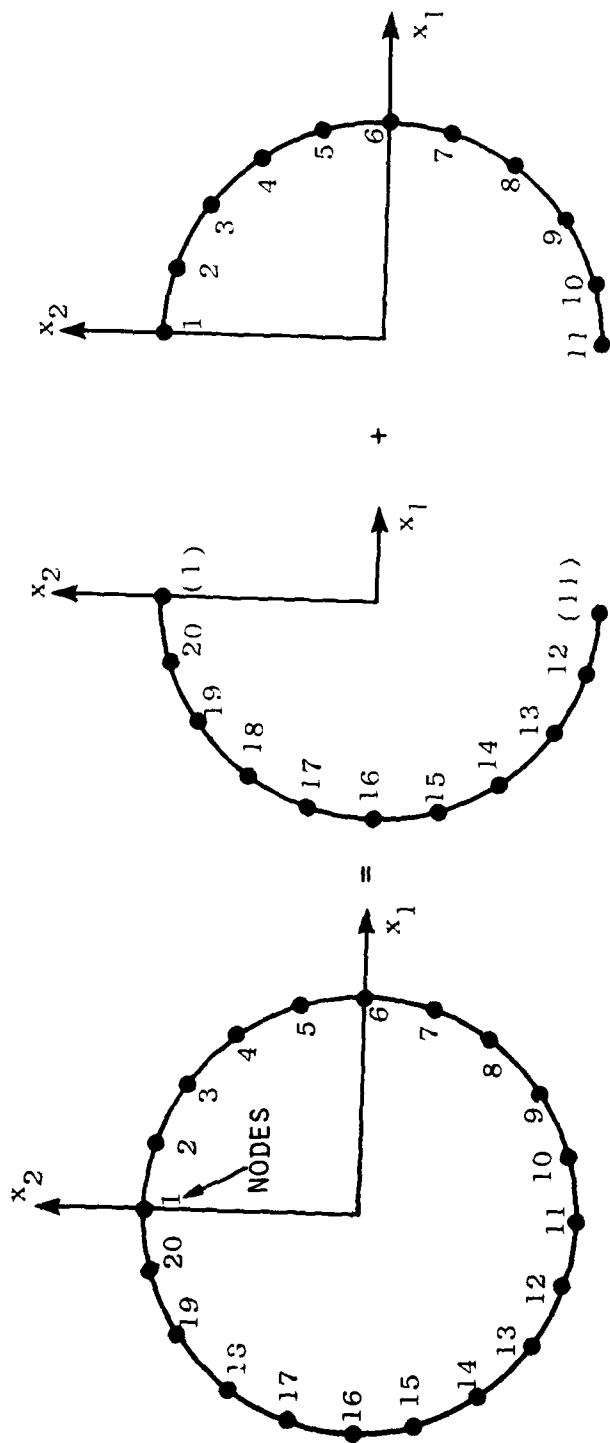
and

$$\underline{F}_r = \underline{F}_{11} + \underline{F}_{12} \underline{T} + \underline{T}^T \underline{F}_{21} + \underline{T}^T \underline{F}_{22} \underline{T}$$

where superscript T indicates matrix transposition. Equations (D-3) may appear to require as much storage for assembly as the full model matrices, but they do not as each of the four terms are assembled individually and stored in \underline{S}_r and \underline{F}_r as they are generated. The stiffness matrix \underline{K}_r for the symmetry model is then formed from

$$\underline{K}_r = \underline{F}_r^{-1} \underline{S}_r \quad (\text{D-4})$$

If a method existed to directly generate the boundary element stiffness without forming \underline{F} and \underline{S} and then solving for \underline{K} the matrix algebra presented could be eliminated. The \underline{K} matrix would simply be assembled for half the problem and the boundary conditions for symmetry imposed, as is done in the finite element method.



e - d.o.f r - d.o.f.

Figure D-1. X_2 -axis of symmetry - example problem.

DISTRIBUTION LIST

DEPARTMENT OF DEFENSE

Assistant to the Secretary of Defense
Atomic Energy
ATTN: Executive Assistant

Defense Advanced Rsch. Proj. Agency
ATTN: TIO

Defense Intelligence Agency
ATTN: RDS-3A
ATTN: DB-4C2, B. Morris

Defense Nuclear Agency
ATTN: DDST
2 cy ATTN: SPSS
4 cy ATTN: TITL

Defense Technical Information Center
12 cy ATTN: DD

Federal Emergency Management Agency
ATTN: Hazard Eval. & Vul. Red. Div.,
G. Sisson

Field Command
Defense Nuclear Agency
ATTN: FCT
ATTN: FCTMOF
ATTN: FCPR

Field Command
Defense Nuclear Agency
Livermore Division
ATTN: FCPRL

Interservice Nuclear Weapons School
ATTN: TTV

Joint Strategic Tgt. Planning Staff
ATTN: NRI-STINFO, Library

NATO School (SHAPE)
ATTN: U.S. Documents Officer

Undersecretary of Defense for Rsch. & Engrg.
ATTN: Strategic & Space Systems (OS)

DEPARTMENT OF THE ARMY

BMD Advanced Technology Center
Department of the Army
ATTN: ATC-T
ATTN: ICRDABH-X

Chief of Engineers
Department of the Army
ATTN: DAEN-RDM
ATTN: DAEN-MCE-D

Construction Engineering Rsch. Lab.
Department of the Army
ATTN: CERL-SOI-L

DEPARTMENT OF THE ARMY (Continued)

Harry Diamond Laboratories
Department of the Army
ATTN: DELHD-I-TL
ATTN: DELHD-N-P

U.S. Army Ballistic Research Labs
ATTN: DRDAR-BLT, A. Ricchiazzi
ATTN: DRDAR-BLT, W. Taylor
ATTN: DRDAR-BLT, C. Kingery
ATTN: DRDAR-BLE, J. Keefer
ATTN: DRDAR-BLV

U.S. Army Communications Command
ATTN: Technical Reference Division

U.S. Army Engr. Waterways Exper. Station
ATTN: Library
ATTN: W. Flathau
ATTN: J. Ballard

U.S. Army War College
ATTN: Library

U.S. Military Academy
ATTN: R. La Frenz

DEPARTMENT OF THE NAVY

David Taylor Naval Ship R & D Ctr.
ATTN: Code 2740
ATTN: Code L42-3, Library
ATTN: Code 1740, R. Short
ATTN: Code 177, E. Palmer
ATTN: Code 1700, W. Murray
ATTN: Code 1740.5

Naval Construction Battalion Center
Civil Engineering Laboratory
ATTN: Code L51, J. Crawford
ATTN: Code L51, R. Odeillo
ATTN: Code L51, S. Takahashi

Naval Ocean Systems Center
ATTN: Code 013, E. Cooper
ATTN: Code 4471

Naval Postgraduate School
ATTN: Code 1424
ATTN: Code 0142

Naval Research Laboratory
ATTN: Code 8440, G. O'Hara
ATTN: Code 8403, R. Belsham
ATTN: Code 8404, H. Pusey
ATTN: Code 2627
ATTN: Code 8440, F. Rosenthal

Naval Sea Systems Command
ATTN: SEA-06J, R. Lane
ATTN: SEA-033
ATTN: SEA-9931G
ATTN: SEA-09G53
ATTN: SEA-0351

DEPARTMENT OF THE NAVY (Continued)

Naval Ship Engineering Center
ATTN: SEC-6105D
ATTN: Code 09G3

Naval Surface Weapons Center
ATTN: Code R14
ATTN: Code R10
ATTN: Code U401, M. Kleinerman
ATTN: Code F31

Naval Weapons Center
ATTN: Code 3263, J. Bowen
ATTN: Code 266, C. Austin
ATTN: Code 233

Office of Naval Research
ATTN: Code 715
ATTN: Code 474, N. Perrone
ATTN: Code 463, J. Heacock

DEPARTMENT OF THE AIR FORCE

Air Force Geophysics Laboratory
ATTN: LWW, K. Thompson

Air Force Institute of Technology, Air University
ATTN: Commander
ATTN: Library

Air Force Office of Scientific Research
ATTN: NA, B. Wolfson

Air Force Weapons Laboratory
Air Force Systems Command
ATTN: DED
ATTN: DES-G, S. Melzer
ATTN: DE, M. Plamondon
ATTN: SUL
ATTN: DES-C, R. Henny

Ballistic Missile Office
Air Force Systems Command
ATTN: DEB

Ballistic Missile Office
Air Force Systems Command
ATTN: MNNH
ATTN: MMH

Headquarters Missile Office
Air Force Systems Command
ATTN: RSS, D. Dowler

Headquarters Space Division
Air Force Systems
Command
ATTN: DYS

Rome Air Development Center
Air Force Systems Command
ATTN: TSLD

Strategic Air Command
Department of the Air Force
ATTN: NRI-STINFO, Library

United States Air Force Academy
ATTN: DFCEM, W. Fluhr

DEPARTMENT OF ENERGY

Department of Energy
ATTN: Document Control for OMA/RD&T

DEPARTMENT OF ENERGY CONTRACTORS

Lawrence Livermore Laboratory
ATTN: Document Control for L-90,
D. Norris
ATTN: Document Control for L-96,
L. Woodruff
ATTN: Document Control for M. Fernandez
ATTN: Document Control for J. Goudreau
ATTN: Document Control for Technical
Information Dept. Library
ATTN: Document Control for J. Thomsen
ATTN: Document Control for L-200,
T. Butkovich
ATTN: Document Control for L-205, J. Hearst
ATTN: Document Control for L-200, J. Cortez
ATTN: Document Control for L-437, R. Schock
ATTN: Document Control for L-90, R. Dong
ATTN: Document Control for T. Gold

Los Alamos Scientific Laboratory
ATTN: Document Control for A. Davis
ATTN: Document Control for T. Dowler
ATTN: Document Control for RMS 364

Sandia Laboratories
Livermore Laboratory
ATTN: Document Control for Library &
Security Classification Div.

Sandia Laboratories
ATTN: Document Control for W. Roherty
ATTN: Document Control for A. Chabai
ATTN: Document Control for W. Herrmann
ATTN: Document Control for 3141

OTHER GOVERNMENT AGENCIES

Department of the Interior
Bureau of Mines
ATTN: Technical Library

Department of the Interior
U.S. Geological Survey
ATTN: D. Roddy

NASA
Ames Research Center
ATTN: R. Jackson

U.S. Nuclear Regulatory Commission
ATTN: R. Whipp for Div. of Security
for L. Shao

DEPARTMENT OF DEFENSE CONTRACTORS

Aerospace Corp.
ATTN: L. Selzer
2 cy ATTN: Technical Information Services

Agabian Associates
ATTN: C. Bagge

DEPARTMENT OF DEFENSE CONTRACTORS (Continued)

Applied Theory, Inc.
2 cy ATTN: J. Trulio

Artec Associates, Inc.
ATTN: S. Gill

Avco Research & Systems Group
ATTN: Library, A830

BDM Corp.
ATTN: Corporate Library

BDM Corp.
ATTN: R. Hensley

Bell Telephone Labs
ATTN: J. White

Boeing Co.
ATTN: Aerospace Library
ATTN: R. Dyrdaahl
ATTN: J. Wooster

California Institute of Technology
ATTN: T. Ahrens

California Research & Technology, Inc.
ATTN: K. Kreyenhagen
ATTN: S. Shuster
ATTN: Library

California Research & Technology, Inc.
ATTN: D. Orphal

Center for Planning & Rsch., Inc.
ATTN: R. Shnider

Civil Systems, Inc.
ATTN: J. Bratton

University of Denver
Colorado Seminary
Denver Research Institute
ATTN: Sec. Officer for J. Wisotski

EG&G Washington Analytical Services Center, Inc.
ATTN: Director

Electric Power Research Institute
Nuclear Power Division
ATTN: G. Sliter

Electromechanical Sys. of New Mexico, Inc.
ATTN: R. Shunk

Eric H. Wang
Civil Engineering Rsch. Fac.
ATTN: N. Baum
ATTN: D. Calhoun

Franklin Institute
ATTN: Z. Zudans

General Dynamics Corp.
ATTN: K. Anderson

DEPARTMENT OF DEFENSE CONTRACTORS (Continued)

General Electric Co.
ATTN: M. Bortner

General Electric Co.
ATTN: A. Ross

General Electric Company-TEMPO
ATTN: DASIAC

General Research Corp.
ATTN: B. Alexander

Geocenters, Inc.
ATTN: E. Marram

H-Tech Labs, Inc.
ATTN: B. Hartenbaum

IIT Research Institute
ATTN: Documents Library
ATTN: A. Longinow

University of Illinois
Consulting Services
ATTN: N. Newmark
ATTN: W. Hall
ATTN: J. Haltiwanger

University of Illinois
ATTN: A. Ang

J. H. Wiggins Co., Inc.
ATTN: J. Collins

Kaman Avidyne
ATTN: Library

Kaman Sciences Corp.
ATTN: Library

Karagozian and Case
ATTN: J. Karagozian

Lockheed Missiles & Space Co., Inc.
ATTN: TIC, Library

Lockheed Missiles and Space Co., Inc.
ATTN: B. Almroth
ATTN: T. Geers
ATTN: P. Underwood

Martin Marietta Corp.
ATTN: A. Cowan

Martin Marietta Corp.
ATTN: J. Donathan

University of Massachusetts
Astronomy Research Facility
ATTN: W. Nash

McDonnell Douglas Corp.
ATTN: R. Halprin

Merritt CASES, Inc.
ATTN: J. Merritt
ATTN: Library

DEPARTMENT OF DEFENSE CONTRACTORS (Continued)

Meteorology Research, Inc.
ATTN: W. Green

Mitre Corp.
ATTN: Director

University of Oklahoma
ATTN: J. Thompson

Pacifica Technology
ATTN: G. Kent
ATTN: R. Bjork
ATTN: R. Allen

Physics International Co.
ATTN: E. Sauer
ATTN: L. Behrmann
ATTN: E. Moore
ATTN: Technical Library

R&D Associates
ATTN: R. Port
ATTN: C. MacDonald
ATTN: J. Lewis
ATTN: Technical Information Center

Rand Corp.
ATTN: Library
ATTN: C. Mow

Science Applications, Inc.
ATTN: Technical Library

Science Applications, Inc.
ATTN: S. Oston

Science Applications, Inc.
ATTN: R. Hoffmann
ATTN: D. Bernstein

Science Applications, Inc.
ATTN: B. Chambers, III

Southwest Research Institute
ATTN: W. Baker
ATTN: A. Wenzel

DEPARTMENT OF DEFENSE CONTRACTORS (Continued)

SRI International
ATTN: G. Abrahamson
ATTN: W. Wilkinson

Systems, Science & Software, Inc.
ATTN: Library
ATTN: T. Cherry
ATTN: T. Riney
ATTN: D. Grine

Teledyne Brown Engineering
ATTN: J. Ravenscraft

Terra Tek, Inc.
ATTN: Library

Tetra Tech, Inc.
ATTN: Library

Texas A & M University System
Texas A & M Research Foundation
ATTN: H. Coyle

TRW Defense & Space Sys. Group
ATTN: Technical Information Center
ATTN: P. Bhutta
ATTN: A. Narevsky
2 cy ATTN: P. Dai

TRW Defense & Space Sys. Group
ATTN: G. Hulcher

Weidlinger Assoc., Consulting Engineers
ATTN: J. McCormick
ATTN: M. Baron

Weidlinger Assoc., Consulting Engineers
ATTN: J. Isenberg

Westinghouse Electric Corp.
ATTN: W. Volz

DATE
ILME